DISEASES AND DISORDERS

Ppp1r3b is a metabolic switch that shifts hepatic energy storage from lipid to glycogen

Kate Townsend Creasy[1,2,3]*, Minal B. Mehta[4], Carolin V. Schneider[2], Joseph Park[4], David Zhang[4], Swapnil V. Shewale[4], John S. Millar[3], Marijana Vujkovic[2], Nicholas J. Hand[4], Paul M. Titchenell[3,5], Joseph A. Baur[3,5]†, Daniel J. Rader[2,3,4]†

The *PPP1R3B* gene, encoding PPP1R3B protein, is critical for liver glycogen synthesis and maintaining blood glucose levels. Genetic variants affecting *PPP1R3B* expression are associated with several metabolic traits and liver disease, but the precise mechanisms are not fully understood. We studied the effects of both *Ppp1r3b* overexpression and deletion in mice and cell models and found that both changes in *Ppp1r3b* expression result in dysregulated metabolism and liver damage, with overexpression increasing liver glycogen stores, while deletion resulted in higher liver lipid accumulation. These patterns were confirmed in humans where variants increasing *PPP1R3B* expression had lower liver fat and decreased plasma lipids, whereas putative loss-of-function variants were associated with increased liver fat and elevated plasma lipids. These findings support that PPP1R3B is a crucial regulator of hepatic metabolism beyond glycogen synthesis and that genetic variants affecting *PPP1R3B* expression levels influence if hepatic energy is stored as glycogen or triglycerides.

INTRODUCTION

Obesity is a growing worldwide epidemic that carries numerous metabolic complications including increased risk of type 2 diabetes (T2D), dyslipidemia, cardiovascular disease, and metabolic dysfunction–associated steatotic liver disease (MASLD, formerly nonalcoholic fatty liver disease or NAFLD). MASLD is a spectrum of liver conditions that includes the initial accumulation of excess triglyceride (TG) in lipid droplets in the liver (steatosis), its progression to inflammatory metabolic dysfunction–associated steatohepatitis, and further to fibrosis, cirrhosis, and hepatocellular carcinoma, with diminishing liver function and increasing risk of comorbidities at each stage. Advanced stages of MASLD are a growing public health concern and are currently among the leading indications for liver transplant due to failure (*1*). MASLD is highly prevalent among patients with obesity (60 to 95%), T2D (55 to 70%), and metabolic syndrome (43 to 67%), and is also highly heritable (*2*, *3*). Investigating the mechanisms and metabolic consequences of genes associated with MASLD and related cardiometabolic disorders may help elucidate the pathophysiology of these disorders to develop better screening and diagnostic criteria as well as therapeutic strategies to address this growing health concern.

Several genome-wide association studies (GWASs) have associated a chromosomal region at 8p23.1, named *PPP1R3B* for the nearest coding gene, with multiple metabolic traits including elevated fasting glucose, insulin, and lactate levels (*4*, *5*), lower plasma lipids (*6*), as well as increased liver enzymes alanine aminotransferase (ALT) and alkaline phosphatase (ALP) (*7*–*9*). A recent large GWAS in the Million Veteran Program (MVP) identified this locus as significantly associated with NAFLD defined by chronically elevated ALT (*9*). The variants at these GWAS signals comprise a tight linkage block with the sentinel single-nucleotide polymorphisms (SNPs) from all relevant GWAS falling within 873 base pairs of one another and overlapping the proximal promoter and 5′ end of a long noncoding RNA (lncRNA) *LOC157273*. The lead SNP associated with increased risk of elevated ALT and lower plasma lipids, rs9987289, was also reported to be a liver expression quantitative trait locus for *PPP1R3B*, with the minor allele associated with higher liver *PPP1R3B* transcript levels (*6*). Because the minor allele is associated with higher fasting glucose, lower plasma lipids, and higher ALT and ALP, this suggested that increased hepatic *PPP1R3B* expression confers these phenotypes. Recent studies support that the *LOC157273* lncRNA is a transcriptional repressor of *PPP1R3B* expression, as carriers of the minor allele have lower abundance of this lncRNA and increased *PPP1R3B* expression, while CRISPR-Cas9 deletion of the rs4841132 SNP region in HuH7 cells leads to decreased *LOC157273* mRNA and increased *PPP1R3B* expression (*10*, *11*). *LOC157273* is expressed in humans and nonhuman primates but is not conserved in rodents (*10*).

The *PPP1R3B* gene encodes the glycogen regulatory protein phosphatase 1 (PP1) regulatory subunit 3B (historically known as G_L). PPP1R3B recruits PP1 to dephosphorylate glycogen synthase (GS), increasing activity, and glycogen phosphorylase (GP), decreasing activity, the rate-limiting enzymes in glycogen synthesis and hydrolysis, respectively, which effectively increases liver glycogen stores (fig. S1) (*12*, *13*). The glycemic and T2D GWAS associations are concordant with the functional roles of PPP1R3B in glycogen metabolism and glucose homeostasis as demonstrated in mouse and cell models (*14*, *15*). However, the mechanisms by which *PPP1R3B* expression is associated with hepatic and plasma lipid metabolism remain unclear. The *PPP1R3B/LOC157273* locus was identified as a signal for hepatic steatosis measured by computed tomography (CT), ultrasound, or magnetic resonance imaging (MRI), although there was no histological evidence of steatosis in matched liver biopsies when evaluated (*8*, *16*, *17*). Subsequent GWAS and mechanistic studies have since provided strong evidence that the *LOC157273* SNPs (with increased *PPP1R3B* expression) are actually a signal for increased hepatic glycogen, which alters liver attenuation and can be ambiguous on

[1]Department of Biobehavioral Health Sciences, School of Nursing, University of Pennsylvania, Philadelphia, PA, USA. [2]Division of Translational Medicine and Human Genetics, Perelman School of Medicine, University of Pennsylvania, Philadelphia, PA, USA. [3]Institute for Diabetes, Obesity, and Metabolism, Perelman School of Medicine, University of Pennsylvania, Philadelphia, PA, USA. [4]Department of Genetics, Perelman School of Medicine, University of Pennsylvania, Philadelphia, PA, USA. [5]Department of Physiology, Perelman School of Medicine, University of Pennsylvania, Philadelphia, PA, USA.
*Corresponding author. Email: creasykt@upenn.edu
†These authors contributed equally to this work.

liver imaging, and that increased glycogen storage contributes to mild liver damage that is reflected in elevated plasma ALT (*10*, *15*, *18*, *19*). Studies in several European population cohorts support that the reported *LOC157273* SNPs have less hepatic lipid accumulation assessed by imaging and that *LOC157273* variant carriers with traditional MASLD risk factors were protected from steatosis (*15*, *18*, *20*). We recently reported concurring findings that the *PPP1R3B/LOC157273* locus is associated with chronically elevated ALT but less hepatic fat estimated by radiological imaging (*9*). *PPP1R3B* is suggested as a T2D therapeutic target, as *PPP1R3B* overexpression and increased hepatic glycogen synthesis improves postprandial glucose clearance from blood (*21*, *22*). Thus, the consequences of altered *PPP1R3B* expression on liver steatosis, hepatic injury, and other metabolic phenotypes have broad implications for human health, but the mechanistic relationship of these genetic variants to hepatic glycogen accumulation, hepatic steatosis, transaminases, and plasma lipids remains uncertain.

The liver is central to the regulation of energy homeostasis, largely through glycogen metabolism. During fasting, liver glycogen stores are used to supply glucose to extrahepatic tissues, and once depleted, the liver relies on lactate and glycerol from TG lipolysis for gluconeogenesis as well as ketogenesis to supply carbon metabolites for adenosine triphosphate (ATP) synthesis (*23*, *24*). In the fed state, carbohydrate derivatives metabolized to glucose replenish hepatic glycogen stores, and then excess metabolites are used for de novo lipogenesis (DNL) and energy storage as TG (*23*, *25*). Given the role of PPP1R3B in regulating hepatic glycogen metabolism (*14*), we investigated the metabolic consequences of both *Ppp1r3b* overexpression and deletion in mouse liver and hepatocyte cell models to elucidate the mechanisms underlying the GWAS associations with liver and metabolic traits at this locus.

RESULTS

Metabolic and liver phenotypes in mice with altered hepatocyte *Ppp1r3b* expression

In the postprandial state, hepatic glucose is rapidly converted to glucose-6-phosphate, which then acts as an allosteric activator of GS to rapidly increase glycogen stores following a fasting period. During prolonged fasting when glycogen stores are depleted, hepatocytes use TG as the primary source of generating ATP (*26*). We previously demonstrated that deletion of *Ppp1r3b* in mouse hepatocytes diminishes the conversion of postprandial glucose into hepatic glycogen, resulting in lower fasting plasma glucose and accelerated activation of gluconeogenic genes (*14*). Since defective glucose-to-glycogen synthesis and increased gluconeogenesis both are associated with hepatic steatosis, we sought to determine the impact of *Ppp1r3b* expression on hepatic TG accumulation. Littermate 8-week-old $Ppp1r3b^{f/f}$ mice were administered hepatocyte-specific [thyroxine-binding globulin (TBG) promoter] adeno-associated virus (AAV) with either *Cre recombinase* for deletion ($Ppp1r3b^{\Delta hep}$), mouse *Ppp1r3b* for overexpression ($Ppp1r3b^{hepOE}$), or empty expression cassette as control ($Ppp1r3b^{f/f}$) and were maintained on chow (fig. S2A). At 4 months of age, $Ppp1r3b^{\Delta hep}$ mice had reduced 4-hour fasting blood glucose compared to both $Ppp1r3b^{f/f}$ and $Ppp1r3b^{hepOE}$ mice [$Ppp1r3b^{f/f}$ (145.2 mg/dl); $Ppp1r3b^{\Delta hep}$ (77.9 mg/dl); $Ppp1r3b^{hepOE}$ (168 mg/dl); Fig. 1A]. There were nonsignificant trends toward increased fasting blood insulin in $Ppp1r3b^{hepOE}$ mice and lowered fasting blood lactate levels in $Ppp1r3b^{\Delta hep}$ mice (Fig. 1, B and C). $Ppp1r3b^{\Delta hep}$ mice had elevated fasting blood ketones [$Ppp1r3b^{f/f}$ (0.46 mM); $Ppp1r3b^{\Delta hep}$ (1.mM); $Ppp1r3b^{hepOE}$ (0.6 mM); Fig. 1D], consistent with lipid oxidation as an alternate fasting energy source. As expected, $Ppp1r3b^{\Delta hep}$ mice had markedly reduced liver glycogen while $Ppp1r3b^{hepOE}$ mice had increased glycogen levels (Fig. 1F), along with increased liver/body weight ratio (Fig. 1E) reflecting increased liver glycogen stores. $Ppp1r3b^{\Delta hep}$ mice had increased liver TG, while $Ppp1r3b^{hepOE}$ mice had decreased liver TG compared with $Ppp1r3b^{f/f}$ mice (Fig. 1G). There was also histological evidence of steatosis in livers from $Ppp1r3b^{\Delta hep}$ mice marked by positive immunohistochemical staining for the lipid droplet–associated protein PLIN2 (Fig. 1, I and K), while $Ppp1r3b^{hepOE}$ livers appeared free of lipid droplets and had increased glycogen deposition visible with Periodic acid–Schiff's (PAS) staining (Fig. 1J). None of the groups had appreciable changes in collagen deposition by Sirius red staining (Fig. 1L). Both the $Ppp1r3b^{\Delta hep}$ and $Ppp1r3b^{hepOE}$ mice had elevated plasma ALT compared to control $Ppp1r3b^{f/f}$ mice (Fig. 1H), indicating that both deletion and overexpression of hepatocyte *Ppp1r3b* contributed to liver injury, with excess liver lipid accumulation in the $Ppp1r3b^{\Delta hep}$ mice and excess liver glycogen in the $Ppp1r3b^{hepOE}$ mice.

Age- and diet-dependent effects on hepatic energy storage in $Ppp1r3b^{\Delta hep}$ and $Ppp1r3b^{OE}$ mice

We proceeded to examine the metabolic consequences of hepatic *Ppp1r3b* deletion and overexpression upon aging (6 to 9 months) or after challenge with a high carbohydrate (sucrose) diet. We found that aged $Ppp1r3b^{\Delta hep}$ mice have impaired glucose disposal assessed by glucose tolerance test (GTT) even while maintaining normal glucose disposal during an insulin tolerance test (ITT) (Fig. 2, A and B). $Ppp1r3b^{\Delta hep}$ mice had severely diminished hepatic glycogen levels as expected (Fig. 2C); however, we observed increased liver TG in the aged $Ppp1r3b^{\Delta hep}$ mice compared to $Ppp1r3b^{f/f}$ controls (Fig. 2, D and E). A similar phenotype was previously reported in mice with liver-specific deletion of GS (gene *Gys2*) with greatly diminished liver glycogenesis in which knockout mice have increased liver TG compared to controls at 7 and 15 months of age but not earlier time points (*27*, *28*). The reciprocal phenotype was seen in aged $Ppp1r3b^{hepOE}$ mice, with improved glucose disposal during GTT (Fig. 2F) and normal glucose lowering in response to insulin (Fig. 2G). $Ppp1r3b^{hepOE}$ mice maintained increased hepatic glycogen stores (Fig. 2H) with a nonsignificant trend toward lower liver TG compared to $Ppp1r3b^{f/f}$ (Fig. 2I).

As PPP1R3B has a critical role in glucose metabolism and glycemic traits, we next evaluated the metabolic responses to changes in hepatic *Ppp1r3b* expression in mice challenged with a high-sucrose diet (HSD, 66% sucrose) for 12 weeks. The $Ppp1r3b^{\Delta hep}$ mice developed dramatically impaired glucose tolerance and insulin resistance compared to $Ppp1r3b^{f/f}$ mice, as measured by GTT and ITT (Fig. 2, J and K). The $Ppp1r3b^{hepOE}$ mice continued to display improved glucose disposal and normal responses to insulin (Fig. 2, O and P). On HSD, the $Ppp1r3b^{\Delta hep}$ mice had negligible liver glycogen (Fig. 2L) and increased hepatic TG compared to $Ppp1r3b^{f/f}$ mice (Fig. 2, M and N). Conversely, on the HSD the $Ppp1r3b^{hepOE}$ mice had increased hepatic glycogen and reduced hepatic TG compared to $Ppp1r3b^{f/f}$ (Fig. 2, Q to S). Thus, deletion of hepatic *Ppp1r3b* increases hepatic TG content and overexpression of hepatic *Ppp1r3b* in mice reduces hepatic lipid accumulation, reciprocal to their effects on hepatic glycogen stores.

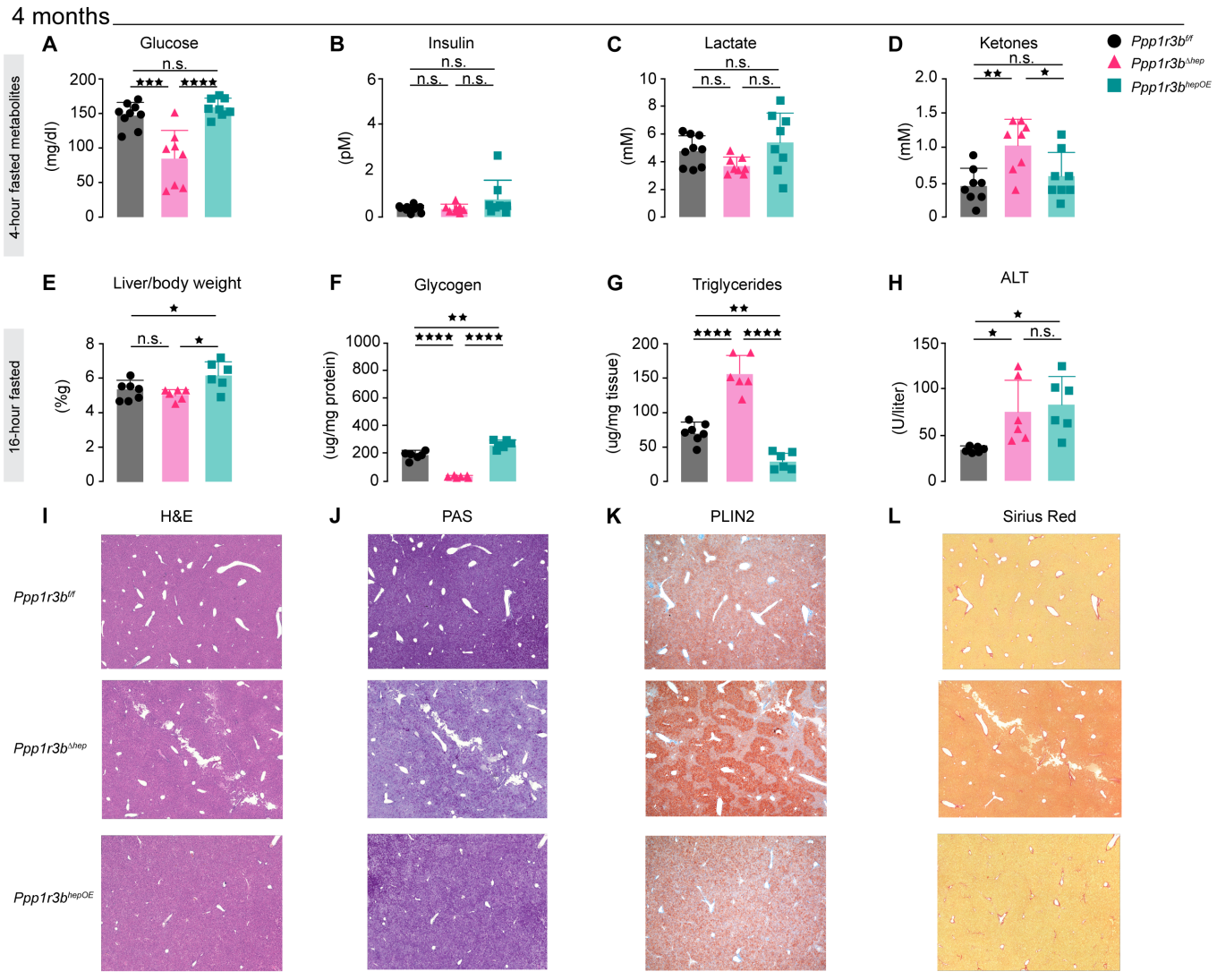

Fig. 1. Mice with hepatocyte *Ppp1r3b* deletion develop metabolic dysfunction contributing to hepatic steatosis with age, while *Ppp1r3b*-overexpressing mice rapidly increase glycogen synthesis and storage contributing to liver damage with aging. Metabolic phenotypes of 4-month-aged mice. (**A** to **D**) Four-hour–fasted metabolites in *Ppp1r3b*$^{f/f}$ (black, $n = 9$), *Ppp1r3b*$^{\Delta hep}$ (pink, $n = 8$), and *Ppp1r3b*^{hepOE} (green, $n = 8$) mice. (A) Blood glucose. (B) Plasma insulin. (C) Blood lactate. (D) Blood ketones. (**E** to **L**) Characteristics of overnight (16 hours)–fasted *Ppp1r3b*$^{f/f}$ (black, $n = 7$), *Ppp1r3b*$^{\Delta hep}$ (pink, $n = 6$), and *Ppp1r3b*^{hepOE} (green, $n = 6$) mice. (E) Liver-to-body weight ratio. (F) Hepatic glycogen content. (G) Hepatic TG content. (H) Fasted plasma ALT measurements. [(I) to (L)] Paraffin-embedded liver sections sectioned and stained with (I) hematoxylin and eosin (H&E), (J) PAS to detect polysaccharide content, (K) immunohistochemistry with PLIN2 antibodies to indicate lipid droplets, and (L) Picro-Sirius Red to detect collagen deposition and liver lesions. Group average presented as bar + SD with individual animals represented as shapes. n.s., not significant.

Effects of hepatocyte *Ppp1r3b* expression on glucose and lipid metabolism

Stender *et al.* (*15*) reported that neither adenovirus-mediated hepatic *Ppp1r3b* overexpression nor *Ppp1r3b* deletion in young chow-fed mice affected hepatic TG levels. Therefore, we next characterized the metabolic phenotypes in young chow-fed mice to better understand the molecular metabolism that could explain the steatosis phenotypes in older and HSD-fed mice we observed. Littermate *Ppp1r3b*$^{f/f}$ mice were administered AAVs at 5 weeks of age and examined after 3 weeks (at 8 weeks of age) and assessed for fasted circulating metabolites. After 4 hours fasting, *Ppp1r3b*^{hepOE} mice maintained higher blood glucose than both *Ppp1r3b*$^{f/f}$ and *Ppp1r3b*$^{\Delta hep}$ mice (Fig. 3A). There were no differences in fasting insulin or lactate (Fig. 3, B and C), but *Ppp1r3b*^{hepOE} mice had reduced fasting blood ketones compared to *Ppp1r3b*$^{f/f}$ and *Ppp1r3b*$^{\Delta hep}$ mice (Fig. 3D). When examined by GTT after an overnight fast, the *Ppp1r3b*^{hepOE} mice had improved glucose disposal, while there was no difference in *Ppp1r3b*$^{\Delta hep}$ mice compared to *Ppp1r3b*$^{f/f}$ (Fig. 3E). The mice were allowed to recover from the GTT and were euthanized at 9 weeks old after an overnight fast. Examination of the livers revealed that *Ppp1r3b*^{hepOE} mice had increased liver-to-body weight ratio (Fig. 3F) and a corresponding increase in glycogen stores (Fig. 3G). The young *Ppp1r3b*$^{\Delta hep}$ mice did not display any differences in liver TG compared to *Ppp1r3b*$^{f/f}$ mice (Fig. 3H) and there were no changes in plasma ALT levels in any of the groups at this age (Fig. 3I), consistent with what had been previously reported (*15*). Livers from *Ppp1r3b*^{hepOE} mice had less

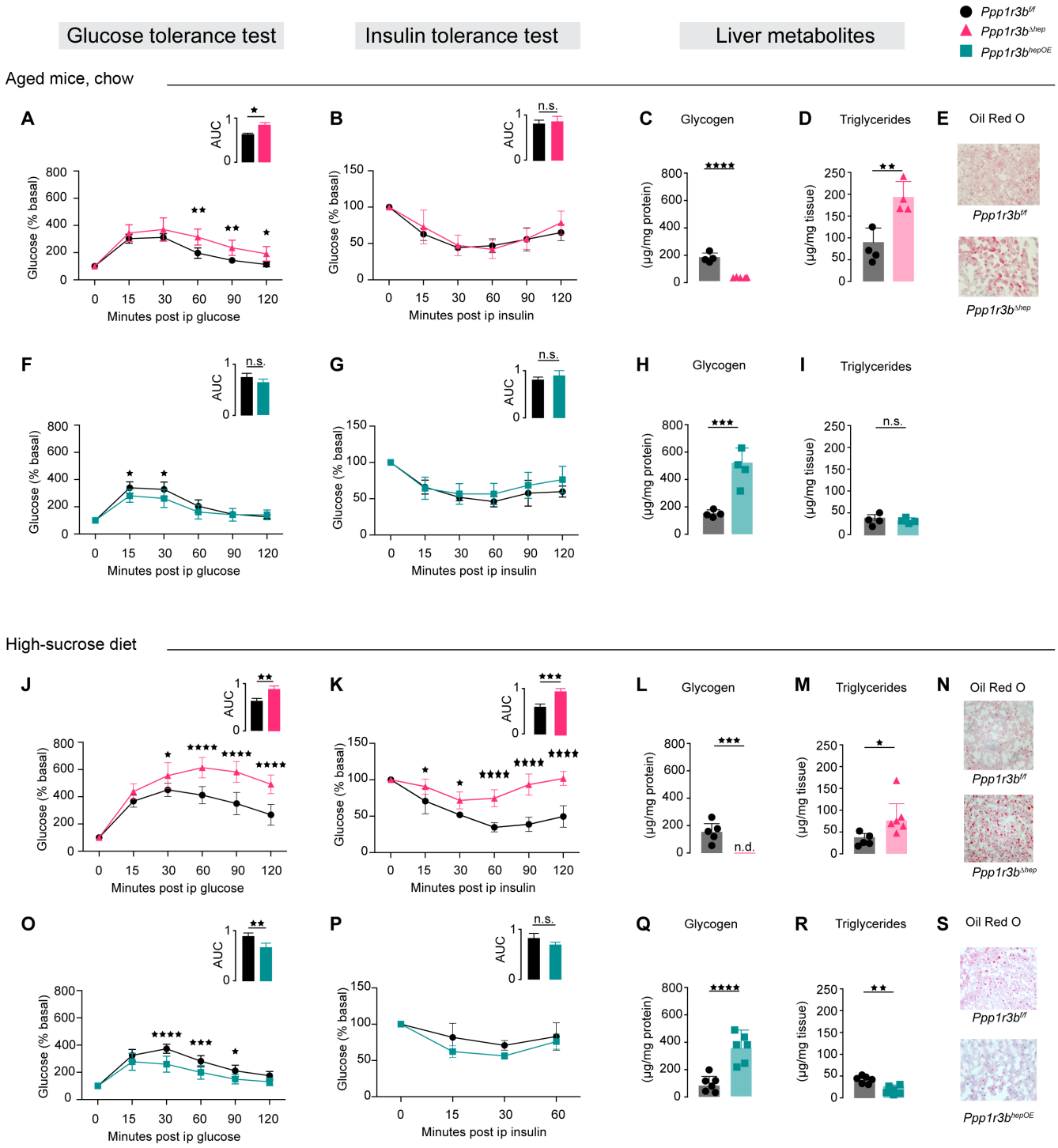

Fig. 2. *Ppp1r3b*$^{\Delta hep}$ mice develop glucose intolerance and steatosis with aging or sucrose diet challenge, while *Ppp1r3b*^{OE} mice have increased liver glycogen and reduced TG content. (**A** to **E**) Metabolic tests performed on fasted 6- to 9-month-aged *Ppp1r3b*$^{f/f}$ (black, $n = 6$) and *Ppp1r3b*$^{\Delta hep}$ (pink, $n = 8$) mice maintained on chow diet. (A) Intraperitoneal (ip) GTT [area under the curve (AUC) inset]. (B) ITT, AUC inset. (C) Hepatic glycogen content. (D) hepatic TG content. (E) Oil Red O staining. (**F** to **I**) Metabolic tests performed on fasted 6- to 9-month-aged *Ppp1r3b*$^{f/f}$ (black, $n = 8$) and *Ppp1r3b*^{hepOE} (green, $n = 6$) mice maintained on chow diet. (F) Intraperitoneal GTT, AUC inset. (G) ITT, AUC inset. (H) Hepatic glycogen content. (I) Hepatic TG content. (**J** to **N**) Metabolic tests performed on fasted *Ppp1r3b*$^{f/f}$ (black, $n = 5$) and *Ppp1r3b*$^{\Delta hep}$ (pink, $n = 7$) mice on HSD (65%) for 12 weeks. (J) Intraperitoneal GTT, AUC inset. (K) ITT, AUC inset. (L) Hepatic glycogen content. (M) hepatic TG content. (N) Oil Red O staining. (**O** to **S**) Metabolic tests performed on fasted *Ppp1r3b*$^{f/f}$ (black, $n = 8$) and *Ppp1r3b*^{hepOE} (green, $n = 8$) on HSD for 12 weeks. (O) Intraperitoneal GTT, AUC inset. (P) ITT, AUC inset. (Q) Hepatic glycogen content. (R) Hepatic TG content. (S) Oil Red O staining. Group average presented as bar + SD with individual animals represented as shapes. n.d., none detected.

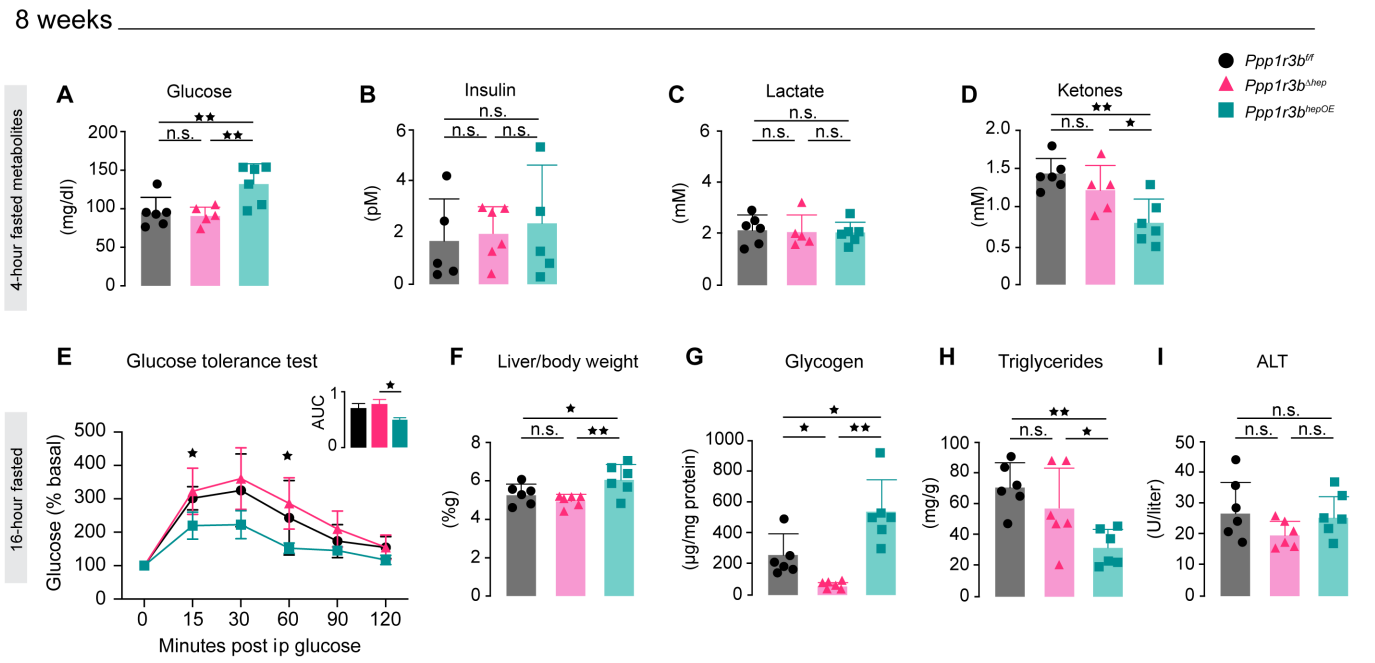

Fig. 3. Changes in hepatocyte *Ppp1r3b* expression alter glucose and lipid metabolism. Young (8 weeks old) mice characterized for metabolic changes in response to hepatic deletion or overexpression of *Ppp1r3b*. (**A** to **D**) Metabolic phenotypes of 8-week-old $Ppp1r3b^{f/f}$ (black, $n = 6$), $Ppp1r3b^{\Delta hep}$ (pink, $n = 6$), and $Ppp1r3b^{hepOE}$ (green, $n = 6$) mice. Four-hour–fasted blood (A) glucose, (B) insulin, (C) lactate, and (D) ketones. (**E** to **I**) Characteristics of overnight (16 hours) fasted $Ppp1r3b^{f/f}$ (black, $n = 6$), $Ppp1r3b^{\Delta hep}$ (pink, $n = 6$), and $Ppp1r3b^{hepOE}$ (green, $n = 6$) mice. (E) Intraperitoneal GTT, AUC inset. (F) Liver-to-body weight ratio. (G) Hepatic glycogen content. (H) Hepatic TG content. (I) Fasted plasma ALT measurements. Group average presented as bar + SD with individual animals represented as shapes.

hepatic TG by both biochemical measurements (Fig. 3H) and histologically (fig. S2B) after 3 weeks of induced *Ppp1r3b* overexpression. These data demonstrate that the metabolic changes and liver phenotypes associated with overexpression of *Ppp1r3b* occur rapidly while hepatic lipid accumulation in $Ppp1r3b^{\Delta hep}$ manifests over time as these phenotypes were only observed in mice 4 months or older or after HSD challenge.

To elucidate the mechanisms underlying the opposing effects on steatosis we observed in $Ppp1r3b^{\Delta hep}$ and $Ppp1r3b^{hepOE}$ mice, we investigated four common pathways that contribute to an imbalance in hepatic lipid accumulation and utilization that are often dysregulated in hepatic steatosis: (i) increased uptake and reesterification of adipose-derived nonesterified fatty acids (NEFA), (ii) increased DNL, (iii) decreased TG secretion in very-low-density lipoprotein (VLDL) particles, and (iv) decreased β-oxidation of lipids. Low blood glucose levels and the corresponding decrease in circulating insulin in acute fasting elicits a cascade of signaling responses to the liver to produce ATP from available sources including glycogenolysis to mobilize hepatic glycogen stores; the use of lactate, glycerol, and amino acids as gluconeogenic substrates; and adipose tissue lipolysis, releasing both glycerol and NEFAs that are taken up by hepatocytes and can be used for β-oxidation or reesterified and stored as TG. The rate of NEFA reesterification typically is greater than β-oxidation resulting in transient steatosis after fasting and with insulin resistance or other metabolic dysfunction contributes to MASLD development (*29*, *30*). Since $Ppp1r3b^{\Delta hep}$ mice have rapid fasting hypoglycemia while $Ppp1r3b^{hepOE}$ mice maintain normal blood glucose levels with extended fasting (*14*), we examined how changes in *Ppp1r3b* expression affected circulating NEFAs. In ad libitum–fed mice, there was no difference in plasma NEFAs among the three groups (Fig. 4A). However, $Ppp1r3b^{\Delta hep}$ mice fasted for 4 hours have elevated plasma NEFAs compared to $Ppp1r3b^{f/f}$ and $Ppp1r3b^{hepOE}$ mice (Fig. 4B). Liver mRNA expression of *Cd36*, the primary transporter of NEFAs in hepatocytes that has been demonstrated to contribute to steatosis (*31*), had a trend toward increased expression in $Ppp1r3b^{\Delta hep}$ mice, while $Ppp1r3b^{hepOE}$ mice have decreased expression compared to $Ppp1r3b^{\Delta hep}$ mice (Fig. 4C), suggesting that $Ppp1r3b^{hepOE}$ mice could have decreased uptake of adipose-derived NEFAs that confers additional protection from steatosis.

In normal liver, postprandial glucose is stored as glycogen for a source of rapid glucose production during short-term fasting or other energy demands. $Ppp1r3b^{\Delta hep}$ mice are unable to store glucose as hepatic glycogen, and we hypothesized that hepatic glucose may be shunted to the DNL pathway resulting in steatosis. We previously reported that $Ppp1r3b^{\Delta hep}$ mice do not exhibit glycogenic compensation by other tissues including skeletal muscle or kidney (*14*), and, therefore, we traced the fate of exogenous glucose in hepatocytes with altered *Ppp1r3b* expression. Primary hepatocytes isolated from 8-weeks-old overnight fasted female mice were labeled with ^{14}C-glucose (1 μCi/ml) for 2 hours, then chased in the label-free media for 2 hours, and then the chase media were assayed for oxidized glucose by measuring radiolabeled CO_2, and cellular lipids were extracted and measured for radiolabeled TG to determine the amount of labeled glucose stored as lipid (*32*). Hepatocytes from $Ppp1r3b^{hepOE}$ mice oxidized more glucose than $Ppp1r3b^{f/f}$ hepatocytes, but there was no difference in the amount of oxidized glucose in $Ppp1r3b^{\Delta hep}$ hepatocytes (Fig. 4D). $Ppp1r3b^{\Delta hep}$ hepatocytes had a dramatic increase in the amount of ^{14}C-glucose glycolytic products converted to DNL production and stored as cellular TG (Fig. 4E). We then assessed in vivo DNL by administering deuterated water

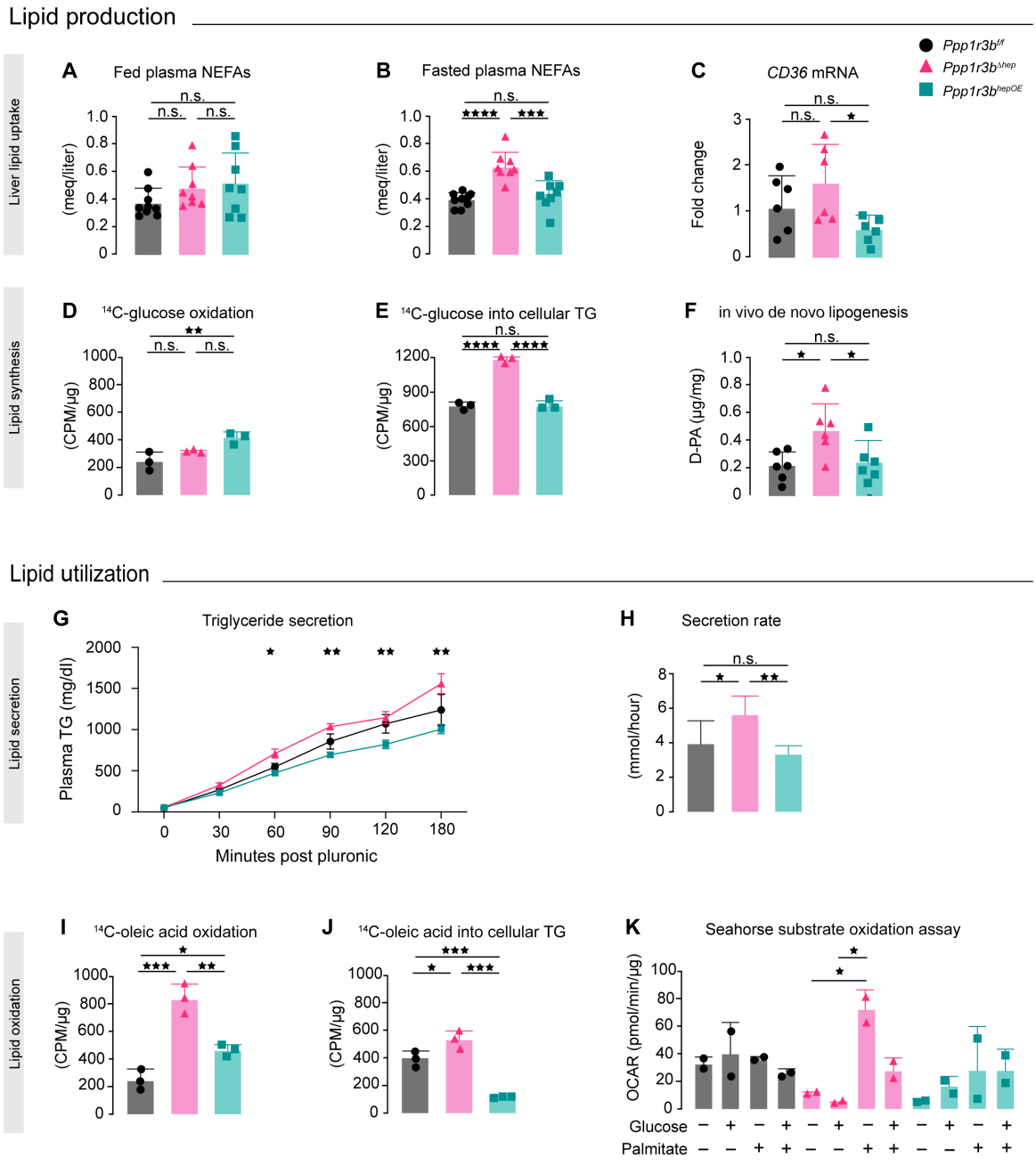

Fig. 4. Altered hepatocyte *Ppp1r3b* expression effects on glucose and lipid metabolism. (**A** to **F**) Lipid accumulation pathways: (A) ad libitum–fed plasma NEFAs. (B) Plasma NEFAs after 4 hours of fasting (*Ppp1r3b*$^{f/f}$ (black, $n = 9$), *Ppp1r3b*$^{\Delta hep}$ (pink, $n = 8$), and *Ppp1r3b*^{hepOE} (green, $n = 8$) mice. (C) Liver mRNA expression levels of lipid transporter *Cd36* in *Ppp1r3b*$^{f/f}$ (black, $n = 6$), *Ppp1r3b*$^{\Delta hep}$ (pink, $n = 6$), and *Ppp1r3b*^{hepOE} (green, $n = 6$) mice. (D) Oxidation of ^{14}C-glucose measured in primary hepatocytes isolated from mice fasted overnight (16 hours). (E) Incorporation of ^{14}C-glucose from media into cellular TG in primary hepatocytes. (F) In vivo DNL assessed by D_2O incorporation into newly synthesized liver palmitate in *Ppp1r3b*$^{f/f}$ (black, $n = 6$), *Ppp1r3b*$^{\Delta hep}$ (pink, $n = 6$), and *Ppp1r3b*^{hepOE} (green, $n = 6$) mice. (**G** to **K**) Lipid utilization pathways: (G) in vivo TG secretion as total plasma concentration and (H) rate of secretion in *Ppp1r3b*$^{f/f}$ (black, $n = 5$), *Ppp1r3b*$^{\Delta hep}$ (pink, $n = 5$), and *Ppp1r3b*^{hepOE} (green, $n = 6$) mice. (I) Oxidation of ^{14}C-oleic acid in primary hepatocytes isolated from mice fasted overnight (16 hours). (J) Incorporation of ^{14}C-oleic acid from media into cellular TG in primary hepatocytes. (K) Seahorse metabolic substrate oxidation assay of primary hepatocytes isolated from fasted *Ppp1r3b*$^{f/f}$ (black, $n = 3$), *Ppp1r3b*$^{\Delta hep}$ (pink, $n = 3$), and *Ppp1r3b*^{hepOE} (green, $n = 3$) mice, tested in either starvation media or supplemented with glucose, palmitate, or both. Oxygen consumption rate (OCR) normalized to microgram protein per well is graphed as an indication of substrate utilization for ATP production. Group average presented as bar + SD with individual animals represented as shapes.

(D_2O) to overnight-fasted mice that were refed for 3 hours and then measured newly synthesized palmitic acid (D_2-PA) in the livers. Consistent with the ex vivo results, the *Ppp1r3b*$^{\Delta hep}$ mice had a significant increase in hepatic D_2-PA compared to both *Ppp1r3b*$^{f/f}$ and *Ppp1r3b*^{hepOE} mice (Fig. 4F).

Even with the changes in glucose utilization and DNL observed in *Ppp1r3b*$^{\Delta hep}$ mice, differences in liver TG were not detected in 8-week-old mice (Fig. 3H), so we next investigated lipid utilization pathways. Hepatocytes export excess lipids from the liver by synthesizing TG and secreting them in VLDL particles, so we tested whether hepatic TG clearance is altered by *Ppp1r3b* expression. TG secretion was measured in fasted 8-week-old mice. *Ppp1r3b*$^{\Delta hep}$ mice displayed increased plasma TG as soon as 1 hour after the start of the assay, and TG were secreted from livers at a faster rate than in *Ppp1r3b*$^{f/f}$ or *Ppp1r3b*^{hepOE} mice (Fig. 4, G and H). Blood metabolites were also measured during this assay, and, as expected, *Ppp1r3b*$^{\Delta hep}$ mice had lower blood glucose levels throughout the experiment (fig. S3A), consistent with our prior reports of hypoglycemia after four or more hours of fasting. There were no changes in blood lactate levels in any of the groups, but *Ppp1r3b*$^{\Delta hep}$ mice had increased blood ketones that were amplified with fasting duration (fig. S3, B and C), suggesting that *Ppp1r3b*$^{\Delta hep}$ mice rely on ketogenesis during fasting to produce energetic substrates, although plasma NEFAs were not different between groups at the terminal time point (fig. S3D). Elevated blood ketones result from β-oxidation of lipids, another lipid clearance mechanism influencing steatosis. We measured the rate of β-oxidation in primary hepatocytes isolated from mice fasted overnight by labeling cells with ^{14}C-oleic acid. *Ppp1r3b*$^{\Delta hep}$ hepatocytes had an increased rate of lipid oxidation when maintained in low-glucose (5.5 mM) media (Fig. 4I). Hepatocytes from *Ppp1r3b*$^{\Delta hep}$ mice also had increased incorporation of the exogenous ^{14}C-oleic acid into cellular lipids (Fig. 4J). Although lower than *Ppp1r3b*$^{\Delta hep}$ hepatocytes, *Ppp1r3b*^{hepOE} cells had increased β-oxidation compared to *Ppp1r3b*$^{f/f}$ cells (Fig. 4I) but had very low incorporation of exogenous lipids into cellular TGs (Fig. 4J). These data support previous findings that the increased liver glycogen in *Ppp1r3b*^{hepOE} mice is sufficient to supply glucose during fasting, and, therefore, the mice are less reliant on β-oxidation for energy than *Ppp1r3b*$^{\Delta hep}$ mice. The increase in β-oxidation compared to *Ppp1r3b*$^{f/f}$ mice was unexpected and may reflect a higher metabolic demand to synthesize more glycogen. Unexpectedly, *Ppp1r3b*$^{\Delta hep}$ cells had increased β-oxidation and cellular TG accumulation simultaneously, indicating the presence of a futile cycle of lipid storage and utilization in *Ppp1r3b*$^{\Delta hep}$ mice. Such futile cycles have been previously described as an early protective adaptation in response to increased hepatic lipid accumulation that may wane with increasing metabolic dysfunction and liver damage (*33*). Increased ketogenesis may metabolize as much as two-thirds of hepatic lipids (*33*), which could explain the lack of steatosis in young, chow-fed *Ppp1r3b*$^{\Delta hep}$ mice, whereas older or HSD-challenged mice have increased liver lipids. These results suggest that although *Ppp1r3b*$^{\Delta hep}$ mice have increased DNL, they also have compensatory changes in hepatic TG utilization during fasting that confer protection against steatosis in young mice with normal feeding conditions. We investigated this possibility in metabolic substrate utilization assays by Seahorse XF substrate oxidation stress test. Primary hepatocytes isolated from overnight fasted (16 hours) mice were assayed for glucose and palmitate oxidation preference. Hepatocytes from *Ppp1r3b*$^{f/f}$ mice had similar maximal mitochondrial respiration rates when the medium was supplemented with glucose (5 mM), palmitic acid (160 μM), or both (Fig. 4K). *Ppp1r3b*$^{\Delta hep}$ hepatocytes preferentially oxidized palmitic acid, and while *Ppp1r3b*^{hepOE} hepatocytes did oxidize exogenous lipids, they more efficiently oxidized glucose (Fig. 4D). The lipid utilization preference observed with *Ppp1r3b* deletion was further supported by improved metabolic profiles in *Ppp1r3b*$^{\Delta hep}$ mice fed a high-fat diet (HFD, 45% lard) for 12 weeks. *Ppp1r3b*$^{\Delta hep}$ mice did not develop insulin resistance and did not have increased hepatic TG compared to *Ppp1r3b*$^{f/f}$ control mice on HFD (fig. S4), as opposed to the severe insulin resistance and steatosis phenotypes observed in *Ppp1r3b*$^{\Delta hep}$ mice on HSD (Fig. 2).

Together, these findings clearly demonstrate that changes in hepatocyte *Ppp1r3b* expression effectively cause a switch between lipid and glucose utilization as energetic substrates. This switch in metabolic efficiencies appears rapidly after changes in *Ppp1r3b* expression, as the metabolic changes are measurable after only 3 weeks of altered hepatic *Ppp1r3b* overexpression. It is intriguing that *Ppp1r3b*$^{\Delta hep}$ mice have a dramatic adaptive response to impaired glycogenesis by storing exogenous glucose as hepatic TG, with a corresponding enhancement in lipid oxidation and TG secretion in fasting conditions. These metabolic changes are present even without differences in total tissue TG accumulation in *Ppp1r3b*$^{\Delta hep}$ mice, and the pericentral lipid droplet accumulation recapitulates early steatosis phenotypes seen in humans. Our data also indicate that both deletion and overexpression of *Ppp1r3b* can result in liver injury, the former presumably due to TG accumulation and the latter presumably to excess glycogen.

Metabolic phenotypes of human *LOC157273/PPP1R3B* variant carriers

Given the results from our mouse models and the replicated associations of altered *PPP1R3B* expression with dysglycemia, plasma lipids, and liver traits in human GWAS, we questioned whether these metabolic dysregulations are present in human carriers of genetic variants at the *PPP1R3B* locus. To clarify the effects of changes in *PPP1R3B* expression on hepatic fat and plasma ALT, we interrogated the Penn Medicine BioBank (PMBB), a large, ethnically diverse biorepository with whole-exome sequencing data, plasma ALT values, and hepatic fat quantifications derived from clinical CT scans using a machine learning approach, for carriers of noncoding variants associated with increased *PPP1R3B* expression and for putative loss-of-function (pLOF) *PPP1R3B* variants. Consistent with published findings, carriers of rs4240624, rs4841132, and rs9987289 (all in strong LD and associated with increased *PPP1R3B* expression) had elevated ALT but decreased hepatic fat estimated by CT attenuation (Fig. 5A). Carriers of *PPP1R3B* pLOF variants were very rare in this dataset ($n = 14$; table S1), which has also been reported by other investigators (*10*) and in the Genome Aggregation Database (gnomAD) (fig. S5). Heterozygous pLOF variant carriers of European ancestry in PMBB had higher CT-derived hepatic fat ($\beta = 20.83$; $P = 0.0012$), and analysis of the rare pLOF variants by gene burden analysis revealed an increased risk of clinical MASLD diagnosis (OR = 8.175, $P = 7.8 \times 10^{-5}$). In addition, *PPP1R3B* pLOF variant carriers of European ancestry have increased abnormal liver function test results (fig. S6). We next identified participants from the UK Biobank who were carriers of either rs4841132-A (increased *PPP1R3B* expression) or *PPP1R3B* pLOF variants and who had plasma metabolomics data available. Heterozygous carriers of rs4841132-A had elevated plasma glucose and reduced plasma lipids and ketones compared to noncarriers, matching the traits and directionality of prior GWAS associations and our

A

Ancestry	Gene/SNP ID	*PPP1R3B* expression	Liver fat (CT attenuation)			ALT (U/liter)		
			Beta	SE	*P* value	Beta	SE	*P* value
EUR	*PPP1R3B* pLOF	↓ (Predicted)	20.83	6.43	***0.001***	−0.01	0.07	0.909
Meta	rs4240624	↑	−1.08	0.21	***5.5E−07***	0.01	0.003	***0.017***
Meta	rs4841132	↑	−1.23	0.24	***5.3E−07***	0.01	0.004	***0.003***
Meta	rs9987289	↑	−1.08	0.21	***6.1E−07***	0.01	0.004	***0.013***

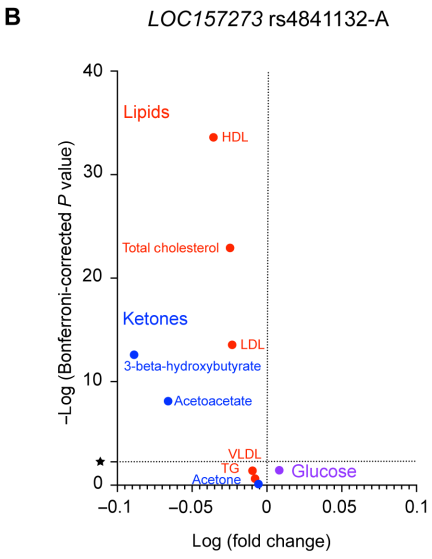

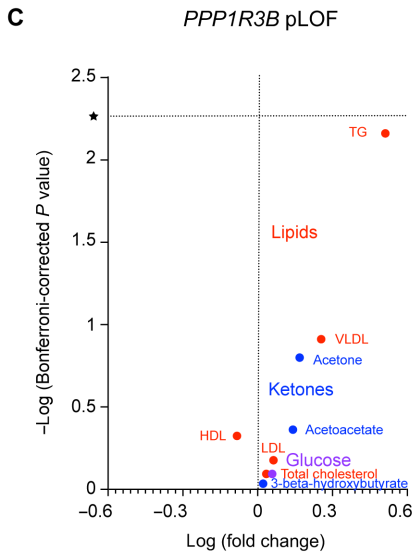

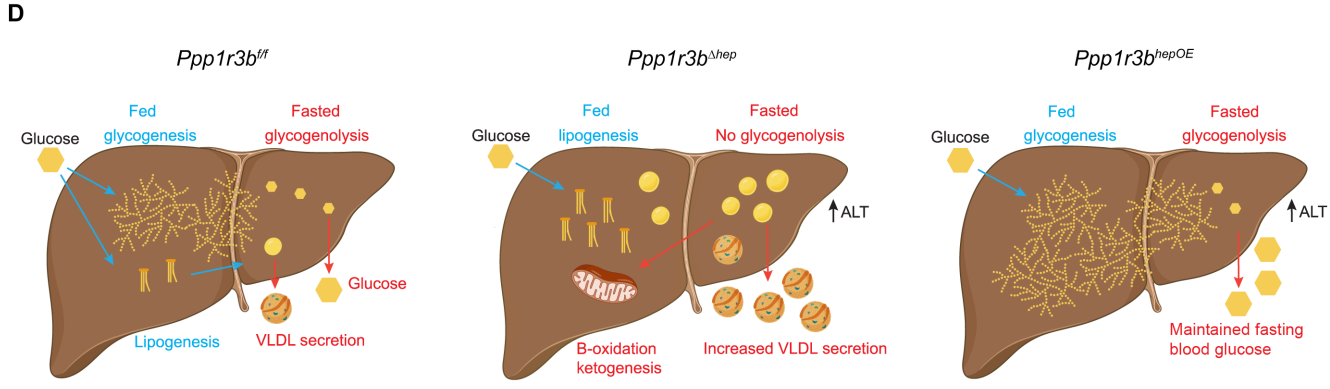

Fig. 5. Characteristics of *LOC157273/PPP1R3B* variant carriers corroborate mouse *Ppp1r3b*$^{\Delta hep}$ and *Ppp1r3b*^{hepOE} phenotypes. (**A**) Analysis of PMBB participants with whole-exome sequencing and CT-derived hepatic fat quantitation yielded a small cohort of individuals with heterozygous *PPP1R3B* pLOF mutations ($n = 14$) as well as carriers of common SNPs in *LOC157273* ($n = 41{,}754$). Beta indicates the direction of effect (>0 indicates increased trait metric, <0 indicates decreased trait metric), SE, standard error; significant *P* values indicated by bold italic font. (**B** and **C**) Plasma metabolomics data from UK Biobank participants with *LOC157273* rs4841132-A SNPs [(B) $n = 17$] and *PPP1R3B* pLOF variants [(C) $n = 25$]. Horizontal line indicates Bonferroni-corrected *P* value with significant metabolites above the line. Vertical line indicates direction of metabolite plasma concentration (>0 indicates increased metabolite; <0 indicates decreased metabolite). (**D**) Model of the effects of altered *Ppp1r3b* expression on liver metabolism. Left, with WT *Ppp1r3b* expression, postprandial glucose is mainly stored as hepatic glycogen with excess glucose stored as TG. In early fasting, glycogen is converted to free glucose to maintain blood glucose levels and meet extrahepatic energy demands, with lipid utilization and TG secretion as VLDL when glycogen is low. Middle, with deletion of hepatocyte *Ppp1r3b* expression, postprandial glycogen synthesis is impaired and exogenous glucose is shunted to lipogenesis and stored as hepatic TG. During fasting, stored TG is oxidized to produce ketones, and lipid is secreted as VLDL. Right, overexpression of hepatocyte *Ppp1r3b* permits enhanced glycogenesis with increased glycogen stores to maintain blood glucose during fasting.

mouse data (Fig. 5B). Heterozygous carriers of *PPP1R3B* pLOF variants exhibited elevated plasma ketones and lipids compared to non-carriers, although the data did not reach significance due to low carrier frequency (Fig. 5C).

DISCUSSION

The *PPP1R3B/LOC157273* locus has been associated with glycemic traits, plasma lipids, and liver traits including elevated plasma ALT and hepatic fat. The encoded protein PPP1R3B is a modulator of hepatic storage of glucose as glycogen with an established molecular role contributing to the glycemic GWAS traits but had unclear mechanistic links to liver lipid metabolism and liver damage phenotypes. Several GWASs have replicated the association of the *LOC157273/PPP1R3B* locus with hepatic steatosis assessed by either CT, ultrasound, or MRI, although there has not been biopsy confirmation of steatosis (*8*, *16*, *17*). Our recent study in the MVP cohort confirmed an association of this locus with steatosis, but in the opposite direction of plasma ALT levels, meaning that *LOC157273/PPP1R3B* variants that increase *PPP1R3B* expression are significantly associated with less hepatic fat measured by CT but still result in liver damage indicated by higher ALT (*9*). Here, we present compelling data demonstrating the role of PPP1R3B in determining hepatic glucose fate in the liver and revealing complex metabolic responses to perturbations in the glycogen metabolism pathway as a result of dysregulated hepatic *Ppp1r3b* expression. With wild-type (WT) *Ppp1r3b* expression, postprandial glucose is stored as hepatic glycogen through glycogenesis (Fig. 5D, left). Upon fasting, glycogenolysis liberates glucose molecules to be exported from the liver to maintain blood glucose levels. Deletion of hepatocyte *Ppp1r3b* in mice results in the inability to store exogenous glucose as glycogen, leading to fasting hypoglycemia and glucose intolerance. During feeding, $Ppp1r3b^{\Delta hep}$ mice shunt glucose to lipogenesis and store energy from both exogenous glucose and lipids as hepatic TG. $Ppp1r3b^{\Delta hep}$ mice appear to rapidly adapt to the lack of glycogen by substituting hepatic TG as a fasting energy source with increased β-oxidation and ketogenesis (Fig. 5D, middle). However, with aging or a high-carbohydrate diet, lipid production, and storage exceed lipid utilization, resulting in steatosis and liver damage indicated by elevated plasma ALT. The reciprocal phenotype is seen in $Ppp1r3b^{hepOE}$ mice, in which increased liver glycogen stores maintain blood glucose during fasting, and glycogen/glucose is the preferred metabolic substrate even with prolonged fasting. $Ppp1r3b^{hepOE}$ mice are protected from hepatic steatosis and do not have altered lipid metabolism in response to fasting or refeeding (Fig. 5D, right). Consequently, the increased hepatic glycogen stores in $Ppp1r3b^{hepOE}$ mice may contribute to glycogenosis with elevated plasma ALT, recapitulating the human phenotypes associated with GWAS SNPs at this locus. Intriguingly, plasma metabolomics in human carriers of rare pLOF mutation in *PPP1R3B* are concordant with the lipid energy preference seen in $Ppp1r3b^{\Delta hep}$ mice, further supporting that PPP1R3B is critical in regulating hepatic glucose storage and consequential energy supply during fasting. These studies provide valuable insights into the role of PPP1R3B as a metabolic switch between hepatic glycogen and lipid storage and demonstrate that changes in *Ppp1r3b* expression, either by deletion or overexpression, contribute to altered glucose metabolism, liver damage, and cardiometabolic disease risk.

PPP1R3B belongs to a family of seven protein phosphatase regulatory proteins (PPP1R3A-G) with differing cell and tissue expression patterns but with the shared function of targeting PP1 to GS for dephosphorylation and enzyme activation (*13*, *34*). PPP1R3B and PPP1R3C (historically "PTG") are the isoforms predominantly expressed in the liver, but PPP1R3B has the unique property of targeting PP1 to both GS and GP to regulate glycogenesis and glycogenolysis (*12*, *13*). We previously reported that hepatocyte *Ppp1r3b* deletion in mice contributes to rapid fasting hypoglycemia and diminished hepatic glycogen stores even in the fed state, while hepatocyte $Ppp1r3b^{hepOE}$ mice have increased liver glycogen stores and maintain prolonged fasting euglycemia (*14*). A subsequent report with constitutive *Ppp1r3b* deletion confirmed the liver glycogen phenotype but reported no changes in liver TG in fed 8-week-old mice (*15*). Liver overexpression of *Ppp1r3b* resulted in increased liver glycogen content but had no effect on liver TG (*15*). This closely resembles phenotypes of human carriers of the minor allele of *LOC157273* SNP rs4841132-A with increased *PPP1R3B* mRNA expression levels who have increased hepatic glycogen without changes in hepatic fat detected by CT attenuation; additional experiments in Huh7 cells with CRISPR-mediated *PPP1R3B* deletion lowered cellular glycogen while *PPP1R3B* overexpression increased glycogen, but no effects on cellular TG were reported (*11*). We also did not detect differences in liver TG in 8-week-old $Ppp1r3b^{\Delta hep}$ mice, although there was a significant reduction in liver TG seen in $Ppp1r3b^{hepOE}$ mice under these conditions. However, with aging or HSD challenge, $Ppp1r3b^{\Delta hep}$ mice have increased liver TG compared to WT mice, and $Ppp1r3b^{hepOE}$ mice continue to have reduced liver TG with HSD. An important distinction between the published studies and our findings is the mouse model used and the timing of the observations: Stender *et al.* (*15*) administered adenovirus to induce *Ppp1r3b* expression and collected samples after 48 hours, whereas we used AAV and collected liver samples after 3 weeks. The Stender *et al.* (*15*) data therefore represent a more acute response to adenovirus treatment, which could explain the elevated ALT and lack of effect on liver TG, whereas our data represent a short-term but adaptive metabolic response to AAV-induced *Ppp1r3b* overexpression. Our glucose tracing studies suggest that although there is no detectable change in liver TG accumulation in young, chow-fed $Ppp1r3b^{\Delta hep}$ mice, there are already metabolic adaptations to the loss of glycogen storage that favor lipid accumulation.

While the effects of *Ppp1r3b* deletion on liver TG accumulation have not been previously reported, similar responses have been demonstrated in other models of dysregulated glycogen metabolism. Mice and primary hepatocytes expressing a *GYS2* mutation that diminishes glycogen synthesis also exhibit increased lipogenesis and liver TG accumulation compared to mice with WT *GYS2* expression (*35*). These findings are consistent in the rare cases of glycogen storage disease type 0 resulting from mutations in *GYS2* with insufficient glycogen synthesis, in which patients have rapid fasting hypoglycemia, increased fasting plasma NEFAs and ketones, and elevated liver enzymes (*36*). In mice with whole-body deletion of *Ppp1r3c* on HFD, there is a decrease in not only liver glycogen but also liver TG (*37*). Conversely, mice with liver-specific overexpression of *Ppp1r3c* largely phenocopy $Ppp1r3b^{hepOE}$ mice, exhibiting increased fasted liver glycogen stores and elevated blood glucose levels, lower fasting NEFAs and ketones, and decreased liver TG (*38*). In a study on the effects of increased liver glycogen stores on exercise endurance, sedentary mice with hepatocyte overexpression of *Ppp1r3c* had lower liver TG compared to WT animals after 16 hours overnight fasting, consistent with our results in $Ppp1r3b^{hepOE}$ mice (*39*). The differences in these models suggest that there are more complex metabolic adaptations to

changes in either *Ppp1r3b* or *Ppp1r3c* expression in a constitutive model compared to the hepatocyte-specific effects that should be further evaluated.

Here, we demonstrate the metabolic consequences of hepatic *Ppp1r3b* overexpression in mice, modeling the common human variants identified by GWAS, as well as hepatocyte *Ppp1r3b* deletion in mice, modeling rare loss-of-function variants in humans, to elucidate the role of *PPP1R3B* in hepatic metabolism underlying the genetic associations with liver and metabolic traits at this locus. Our study has several limitations that should be considered. Characterization of humans with *PPP1R3B* pLOF variants is greatly limited by the scarcity of carriers in the biobank populations we examined, which has also been reported in other biobanks and study populations (*10*, *11*, *15*). It is possible that impaired *PPP1R3B* expression affects survivability and contributes to the low carrier frequency. This observation is recapitulated in mouse models of constitutive deletion of either *Ppp1r3b* or *Ppp1r3c* in which homozygous deletion is observed in less than 25% of offspring from heterozygous breeding pairs (*15*, *37*). A recent study in neonatal mice demonstrated an early postnatal metabolic demand for liver glycogen before a switch to reliance on lipids for energy (*40*), and perhaps the lack of hepatic GS activity through either *Ppp1r3b* or *Ppp1r3c* deletion contributes to neonatal lethality. Together, these observations suggest an important role for *PPPP1R3B* expression for survivability and future studies investigating the metabolic consequences of *PPP1R3B* deficiency and impaired glycogen metabolism during developmental and neonatal stages are warranted. The scarcity of *PPP1R3B* pLOF variant carriers also limits our ability to evaluate the effects on hepatic steatosis with histological grading of human liver biopsies. Our conclusion that *PPP1R3B* pLOF variants increase steatosis in humans (Fig. 5A) is supported by reported changes in CT attenuation that implicate hepatic fat accumulation (*41*). In addition, metabolic adaptations in response to changes in energetic substrate availability can have both acute and chronic effects that present differently on the basis of the timing of experimentation and the length of fasting/feeding cycles as well as the extent of exposure to dietary challenges. We did not measure the rates of DNL, TG secretion, or substrate oxidation in older mice, which could reveal additional metabolic adaptations to the changes in *Ppp1r3b* expression and have consequences on TG accumulation. Several of our experiments were performed ex vivo in primary hepatocytes to tightly control nutrient exposure periods, which limits the interpretation of results compared to an intact biological system with integrated responses from other cell types and tissues. Further, the exact cellular mechanisms of hepatocyte *Ppp1r3b* regulation of glucose and lipid metabolism in response to changes in feeding/fasting and energy sources are not yet fully elucidated. We have recently described a role for mTORC1 promotion of *Ppp1r3b* expression in response to feeding and insulin signaling (*42*), but additional studies are needed to understand the downstream effects on DNL and glycogenic gene expression and hepatic energy storage.

MATERIALS AND METHODS

Generation of hepatocyte-specific Ppp1r3b knockout and overexpressing mice

Mice with hepatocyte-specific deletion ($Ppp1r3b^{\Delta hep}$) and overexpression ($Ppp1r3b^{hepOE}$) were achieved as previously described (*14*). Briefly, $Ppp1r3b^{f/f}$ mice on C57BL/6J background produced for Merck by Taconic were bred to mice expressing Cre recombinase driven by the albumin promoter (*Alb-Cre*), with littermate mice without *Alb-Cre* transgene expression used as controls. *Ppp1r3b* overexpression was induced by administering AAV serotype 8 with TBG promoter–driven murine *Ppp1r3b* [AAV8.TBG.Ppp1r3b; titer 1×10^{12} gc (genomic copies)], and littermates were administered AAV with an empty expression cassette as control (AAV8.TBG.Null; titer 1×10^{12} gc). In some experiments, $Ppp1r3b^{f/f}$ mice were administered AAV with TBG promoter–driven Cre recombinase expression (AAV8.TBG.Cre; titer 1.5×10^{11} gc) to generate hepatocyte-specific *Ppp1r3b* knockout mice. Littermates were administered either AAV8.TBG.Ppp1r3b for overexpression or AAV8.TBG.Null as control (both titers 1.5×10^{11} gc). AAV vectors were generated by the University of Pennsylvania Vector Core (Philadelphia, PA, USA). Both male and female mice were assessed unless specifically indicated.

Animal housing and diet

Animals were housed under controlled temperature (23°C) and lighting (12-hour light/dark cycle) with free access to water and standard mouse chow (LabDiet, 5010), or animals were administered HSD (66.6% kCal sucrose content, Research Diets, D11725i) or HFD (45% kCal lard, Research Diets, D12451i) for 12 weeks. All animal experiments were reviewed and approved by Institutional Animal Care and Use Committee and the University Laboratory Animal Resources Committee of the University of Pennsylvania, Philadelphia, USA, under protocol #804590.

In vivo metabolic testing

For GTT, mice were fasted overnight (14 to 16 hours) and then administered fasted body mass glucose (2 g/kg) by intraperitoneal injection with subsequent measurements of veinous tail blood glucose with a OneTouch Ultra Mini glucometer (LifeScan) at the indicated time points. ITT were performed in mice after 6 hours of fasting by intraperitoneal administration of recombinant insulin (Novolin R; Novodisk A/S; 0.75 U/kg body mass) and subsequent measurement of veinous tail blood glucose with a OneTouch Ultra Mini glucometer (LifeScan) at the indicated time points.

In vivo DNL

Mice were fasted overnight (16 hours) and then weighed, and a baseline blood collection was obtained from retro-orbital bleeding. The mice were administered D_2O (Sigma-Aldrich; 400 μl/20 g body mass) and allowed to feed ad libitum for 3 hours. The mice were then euthanized, and approximately 100 mg of liver tissue and 50 μl of plasma were provided to the Institute of Diabetes, Obesity, and Metabolism Metabolic Tracer Resource at the University of Pennsylvania for analysis of body water and palmitate deuterium enrichment by gas chromatography–electron impact ionization mass spectrometry and subsequent calculation of DNL (*43*).

In vivo TG secretion

Hepatic TG secretion was assessed as previously described (*44*). Male mice were fasted for 4 hours and then administered Pluronic P407 [30 mg in 200 μl of 1× phosphate-buffered saline (PBS)] retro-orbitally under isoflurane anesthesia, and then blood was collected from the retro-orbital vein while under isoflurane anesthesia at the indicated time points. Plasma TG content was measured colorimetrically using Infinity Triglyceride Reagent (Thermo Fisher Scientific) according to the manufacturer's protocol. Hepatic TG secretion rates were calculated from the slope of the regression line of the time versus plasma TG.

Blood and plasma metabolites

Blood glucose, lactate, and ketone bodies were measured in veinous tail blood by OneTouch Ultra Mini glucometer (LifeScan), Lactate Plus (Nova Biomedical), or novaMax Plus (Nova Biomedical) meters, respectively. Plasma insulin was measured by enzyme-linked immunosorbent assay (ChrystalChem, catalog no. 90080). Plasma NEFA and ALT were measured by ACE Alfa Wasserman Axcel autoanalyzer using commercially available colorimetric assay kits (Wako).

Metabolic and biochemical measurements

Hepatic TGs were measured colorimetrically using Infinity Triglyceride Reagent (Thermo Fisher Scientific). Tissues were homogenized in PBS, diluted 1:5, incubated with 1% deoxycholate, and then assayed according to the manufacturer's protocol. Sample TG was calculated by standard curve and normalized to wet tissue mass. Hepatic glycogen levels were measured by Glycogen Assay Kit II (Colorimetric) from Abcam (catalog no. ab169558). Tissues were homogenized with distilled H_2O on ice and then boiled for 10 min. Homogenates were spun at 13,000 r.p.m. for 10 min, and supernatants were assayed for glycogen content. Results were normalized by protein content.

Histology and immunohistochemistry

Tissue sections were paraffin-embedded, sectioned, and stained by the Histology and Gene Expression Co-Op at Penn Cardiovascular Institute. Standard techniques were applied to stain tissues with hematoxylin and eosin to assess general tissue morphology, PAS to detect polysaccharide content, and Picro-Sirius Red to detect collagen deposition and liver lesions. Immunohistochemistry was performed on deparaffinized sections to detect lipid droplets with PLIN2 antibodies (Sigma-Aldrich, HPA016607). Brightfield images were captured on a slide scanning microscope (Keyence, BZ-X800) with 4× objective lens. Lipid droplet accumulation was assessed in frozen liver sections by Oil Red O staining: Fresh liver tissues were embedded in O.C.T. compound (Sakura Finetak), snap frozen, and stored at −80°C. Cryosections were prepared at 10 μm onto slides, fixed in 4% formalin, and stained with Oil-Red-O solution by the Pathology Core Laboratory, Research Institute at Children's Hospital of Philadelphia, Philadelphia, PA, USA). Images were captured using a Nikon Digital Sight DS-U3 camera on Nikon Eclipse 80i microscope with NIS-Elements-D software version 4.12.01.

RNA isolation and quantitative reverse transcription PCR

Total RNA was extracted from approximately 100 mg flash-frozen liver tissue following homogenization in RNAzol RT reagent (Sigma-Aldrich). cDNA was synthesized from 1 μg RNA using High-Capacity cDNA Reverse Transcription Kit (Applied Biosystems). Quantitative real-time polymerase chain reaction (PCR) was performed with SYBR Green Mix (Applied Biosystems) on an QuantStudio 7 Flex Real-Time PCR System (Thermo Fisher Scientific). Oligonucleotide primer sequences used are *Cd36* (forward: AAAGTTGCCATAATTGAGTCCT, reverse: AAAGTTGCCATAATTGAGTCCT), *Ppp1r3b* (forward: AGCCGTACAATGGACCAGAT, reverse: AGTAGTAGGGCCCCAGCTTT), and reference genes *L30* (forward: ATGGTGGCCGCAAAGAAGACGAA, reverse: CCTCAAAGCTGGACAGTTGTTGGCA) and *Hprt* (forward: TGACACTGGCAAAACAATGCA, reverse: GGTCCTTTTCACCAGCAAGCT). The fold change in the target mRNA abundance with respect to the control group and normalized by the geometric mean of the reference genes was calculated using the $2^{-\Delta\Delta C}{}_T$ method and is displayed as fold change in expression compared to the control group.

Primary hepatocyte isolation and ex vivo oxidation assays

Primary hepatocytes were isolated from overnight fasted (16 hours) female mice by a two-step perfusion with collagenase digestion as described previously (*45*). Primary hepatocytes were seeded at a density of 5×10^5 cells per well in triplicate wells of six-well plates. After 2 hours of attachment in glucose-free Dulbecco's modified Eagle's medium, the cells were washed and labeled with either ^{14}C-oleic acid (1 μCi/ml) for β-oxidation or ^{14}C-glucose (1 μCi/ml) for glucose oxidation (*32*, *46*). After 2 hours, the label media were removed and the cells gently washed and chased for 2 hours. The chase media were transferred to sealed oxidation flasks and treated with 70% perchloric acid with gentle rocking for 1 hour to capture ^{14}C-CO_2 on KOH-soaked filter paper. The filter paper and incompletely oxidized intermediates (acid-soluble metabolites) were counted for radioactivity. The cells were washed and lipids extracted by 3:2 hexane:isopropanol, then dried and resuspended in 100% hexane for separation by thin layer chromatography, and the TG bands were cut and counted for radioactivity. The cells were then washed, and cellular protein solubilized and quantified by bicinchoninic acid assay (BCA) to normalize the radioactivity measurements for each well.

Measurement of substrate oxidation by Seahorse analysis

The Seahorse Bioscience XF96 Extracellular Flux analyzer (Agilent) was used to quantify mitochondrial respiration of primary hepatocytes in the presence of nutrient-free media or media supplemented with glucose, palmitic acid, or both. The cells were seeded at 12×10^3 cells per well in 96-well XF96 plates and incubated in nutrient-free media for 1 hour. After the cells adhered, the media were gently aspirated and replaced with either nutrient-free media, glucose media (5 mM glucose), lipid media (160 μM bovine serum albumin–palmitic acid), or combined glucose and lipid media. The cells were incubated for 4 hours, then gently washed, and Seahorse assay media added (180 μl per well) and incubated at 37° without CO_2 for 45 min. The substrate oxidation assay was performed with automated addition of ATP synthase inhibitor (1.5 μM oligomycin), proton uncoupler (2 μM carbonyl cyanide ptrifluoromethoxyphenylhydrazone), and electron transport chain inhibitors (0.5 μM rotenone/antimycin A mixture). At completion of the assay, cellular protein was precipitated by treatment with 0.1 N NaOH and then measured by BCA. The oxygen consumption rates were measured and analyzed using Seahorse Wave software, and normalized to microgram per protein per well.

Analysis of LOC157273 SNPs and PPP1R3B predicted loss-of-function variants in PMBB

All individuals recruited for the PMBB are patients of clinical practice sites of the University of Pennsylvania Health System. This study was approved by the Institutional Review Board of the University of Pennsylvania and complied with the principles set out in the Declaration of Helsinki. PMBB participants who had both whole-exome sequence data and CT-derived hepatic fat quantitation ($n = 10{,}283$) were analyzed for carriage of the *LOC157273* SNPs rs4240624, rs4841132, and rs9987289, or for rare (minor allele frequency <0.1% in gnomAD) pLOF variants and rare predicted deleterious (REVEL >0.8) missense (pDM) variants in *PPP1R3B*, in the genetic region chr8:8997073-9009084 of GRCH38 (*47*, *48*). Analysis of each of the

LOC157273 SNPs and a gene burden of rare pLOF and pDM variants in *PPP1R3B* were associated with hepatic fat using a linear regression model adjusted for age, genetically determined sex, and principal components (PCs) of ancestry (PC1–5 in Africans and PC1–10 in Europeans). We used an additive genetic model to aggregate variants as previously described (*49*). These analyses were performed separately by African and European genetic ancestry and combined with inverse variance weighted meta-analysis.

Phenome-wide association of hepatic fat with EHR diagnoses and traits

A phenome-wide association study (PheWAS) was performed to determine the phenotypes associated with the quantitative trait of median hepatic fat in PMBB for the 10,283 unrelated individuals in PMBB with both exome sequences and quantitated hepatic fat available (*50*). ICD-10 encounter diagnoses were mapped to ICD-9 via the Center for Medicare and Medicaid Services 2017 General Equivalency Mappings (https://cms.gov/medicare/coding-billing/icd-10-codes/icd-10-cm-icd-10-pcs-gem-archive) and manual curation. Phenotypes for each individual were then determined by mapping ICD-9 codes to distinct disease entities (i.e., Phecodes) using the R package "PheWAS" (*51*). Patients were determined to have a certain disease phenotype if they had the corresponding ICD diagnosis on two or more dates, while phenotypic controls consisted of individuals who never had the ICD code. Individuals with an ICD diagnosis on only one date as well as individuals under control exclusion criteria based on PheWAS phenotype mapping protocols were not considered in statistical analyses. Each Phecode was tested for association with quantitated hepatic fat using a logistic regression model adjusted for age, sex, and PCs (PC1-10) of genetic ancestry. The association analyses considered only disease phenotypes with at least 20 cases based on power calculations in a prior simulation study (*49*). This led to the interrogation of 1396 total Phecodes, and we used a Bonferroni correction to adjust for multiple testing ($P = 0.05/1396 = 3.58 \times 10^{-05}$).

Plasma metabolomics in UK Biobank participants

The UK biobank is a population-based cohort study conducted in the United Kingdom from 2006 to 2010, which recruited 502,500 volunteers aged 37 to 73 years at baseline. All participants were registered with the UK National Health Service and attended an initial examination, which is followed by a long-term follow-up taking place continuously. On the baseline visit, blood samples were taken, and biometric measures were performed. In a subgroup of UK biobank participants ($n = 105{,}348$), nuclear magnetic resonance–based plasma metabolomic profiling was performed. Only participants with genetic information and metabolomic profiling were included in the analyses. Plasma glucose, ketone bodies, and major lipid classes were chosen a priori for further analysis. Each metabolite was divided by its SD and calculated the log fold change between variant carriers and controls as well as a −log transformed logistic regression. Differences were considered to be statistically significant when $P < 0.05$. Bonferroni correction was performed to avoid first type of error occurring through multiple testing of $n = 9$ metabolites ($P < 0.05/9 = 0.0056$). The data were analyzed using R version 4.0.2 (R Foundation for Statistical Computing; Vienna, Austria), SPSS Statistics version 26 (IBM; Armonk, NY, USA), and Prism version 8 (GraphPad, LaJolla, CA, USA).

Statistical analyses

All results are presented as means ± SD unless otherwise indicated. Data are presented as one representative experiment, and each experiment was repeated two to three times with consistent outcomes. Results were analyzed by the unpaired two-tailed Student's *t* test or one-way analysis of variance (ANOVA) as appropriate using GraphPad Prism Software (Version 9.3.1, GraphPad Software, Inc.). Statistical significance was defined as $^{*}P < 0.05$, $^{**}P < 0.01$, $^{***}P < 0.001$, $^{****}P < 0001$.

Supplementary Materials

This PDF file includes:

Figs. S1 to S6

Table S1

REFERENCES AND NOTES

1. Z. M. Younossi, M. Stepanova, J. Ong, G. Trimble, S. AlQahtani, I. Younossi, A. Ahmed, A. Racila, L. Henry, Nonalcoholic steatohepatitis is the most rapidly increasing indication for liver transplantation in the United States. *Clin. Gastroenterol. Hepatol.* **19**, 580–589.e5 (2021).
2. A. F. Godoy-Matos, W. S. Silva Júnior, C. M. Valerio, NAFLD as a continuum: From obesity to metabolic syndrome and diabetes. *Diabetol. Metab. Syndr.* **12**, 60 (2020).
3. S. Sookoian, C. J. Pirola, Genetic predisposition in nonalcoholic fatty liver disease. *Clin. Mol. Hepatol.* **23**, 1–12 (2017).
4. A. K. Manning, M.-F. Hivert, R. A. Scott, J. L. Grimsby, N. Bouatia-Naji, H. Chen, D. Rybin, C.-T. Liu, L. F. Bielak, I. Prokopenko, N. Amin, D. Barnes, G. Cadby, J.-J. Hottenga, E. Ingelsson, A. U. Jackson, T. Johnson, S. Kanoni, C. Ladenvall, V. Lagou, J. Lahti, C. Lecoeur, Y. Liu, M. T. Martinez-Larrad, M. E. Montasser, P. Navarro, J. R. B. Perry, L. J. Rasmussen-Torvik, P. Salo, N. Sattar, D. Shungin, R. J. Strawbridge, T. Tanaka, C. M. van Duijn, P. An, M. de Andrade, J. S. Andrews, T. Aspelund, M. Atalay, Y. Aulchenko, B. Balkau, S. Bandinelli, J. S. Beckmann, J. P. Beilby, C. Bellis, R. N. Bergman, J. Blangero, M. Boban, M. Boehnke, E. Boerwinkle, L. L. Bonnycastle, D. I. Boomsma, I. B. Borecki, Y. Böttcher, C. Bouchard, E. Brunner, D. Budimir, H. Campbell, O. Carlson, P. S. Chines, R. Clarke, F. S. Collins, A. Corbatón-Anchuelo, D. Couper, U. de Faire, G. V. Dedoussis, P. Deloukas, M. Dimitriou, J. M. Egan, G. Eiriksdottir, M. R. Erdos, J. G. Eriksson, E. Eury, L. Ferrucci, I. Ford, N. G. Forouhi, C. S. Fox, M. G. Franzosi, P. W. Franks, T. M. Frayling, P. Froguel, P. Galan, E. de Geus, B. Gigante, N. L. Glazer, A. Goel, L. Groop, V. Gudnason, G. Hallmans, A. Hamsten, O. Hansson, T. B. Harris, C. Hayward, S. Heath, S. Hercberg, A. A. Hicks, A. Hingorani, A. Hofman, J. Hui, J. Hung, M.-R. Jarvelin, M. A. Jhun, P. C. D. Johnson, J. Wouter Jukema, A. Jula, W. H. Kao, J. Kaprio, S. L. R. Kardia, S. Keinanen-Kiukaanniemi, M. Kivimaki, I. Kolcic, P. Kovacs, M. Kumari, J. Kuusisto, K. O. Kyvik, M. Laakso, T. Lakka, L. Lannfelt, G. M. Lathrop, L. J. Launer, K. Leander, G. Li, L. Lind, J. Lindstrom, S. Lobbens, R. J. F. Loos, J. Luan, V. Lyssenko, R. Mägi, P. K. E. Magnusson, M. Marmot, P. Meneton, K. L. Mohlke, V. Mooser, M. A. Morken, I. Miljkovic, N. Narisu, J. O'Connell, K. K. Ong, B. A. Oostra, L. J. Palmer, A. Palotie, J. S. Pankow, J. F. Peden, N. L. Pedersen, M. Pehlic, L. Peltonen, B. Penninx, M. Pericic, M. Perola, L. Perusse, P. A. Peyser, O. Polasek, P. P. Pramstaller, M. A. Province, K. Räikkönen, R. Rauramaa, E. Rehnberg, K. Rice, J. I. Rotter, I. Rudan, A. Ruokonen, T. Saaristo, M. Sabater-Lleal, V. Salomaa, D. B. Savage, R. Saxena, P. Schwarz, U. Seedorf, B. Sennblad, M. Serrano-Rios, A. R. Shuldiner, E. J. G. Sijbrands, D. S. Siscovick, J. H. Smit, K. S. Small, N. L. Smith, A. V. Smith, A. Stančáková, K. Stirrups, M. Stumvoll, Y. V. Sun, A. J. Swift, A. Tönjes, J. Tuomilehto, S. Trompet, A. G. Uitterlinden, M. Uusitupa, M. Vikström, V. Vitart, M.-C. Vohl, B. F. Voight, P. Vollenweider, G. Waeber, D. M. Waterworth, H. Watkins, E. Wheeler, E. Widen, S. H. Wild, S. M. Willems, G. Willemsen, J. F. Wilson, J. C. M. Witteman, A. F. Wright, H. Yaghootkar, D. Zelenika, T. Zemunik, L. Zgaga, DIAbetes Genetics Replication And Meta-analysis (DIAGRAM) Consortium, The Multiple Tissue Human Expression Resource (MUTHER) Consortium, N. J. Wareham, M. I. McCarthy, I. Barroso, R. M. Watanabe, J. C. Florez, J. Dupuis, J. B. Meigs, C. Langenberg, A genome-wide approach accounting for body mass index identifies genetic variants influencing fasting glycemic traits and insulin resistance. *Nat. Genet.* **44**, 659–669 (2012).
5. A. Tin, P. Balakrishnan, T. H. Beaty, E. Boerwinkle, R. C. Hoogeveen, J. H. Young, W. H. L. Kao, *GCKR* and *PPP1R3B* identified as genome-wide significant loci for plasma lactate: The Atherosclerosis Risk in Communities (ARIC) study. *Diabet. Med.* **33**, 968–975 (2016).
6. T. M. Teslovich, K. Musunuru, A. V. Smith, A. C. Edmondson, I. M. Stylianou, M. Koseki, J. P. Pirruccello, S. Ripatti, D. I. Chasman, C. J. Willer, C. T. Johansen, S. W. Fouchier, A. Isaacs, G. M. Peloso, M. Barbalic, S. L. Ricketts, J. C. Bis, Y. S. Aulchenko, G. Thorleifsson, M. F. Feitosa, J. Chambers, M. Orho-Melander, O. Melander, T. Johnson, X. Li, X. Guo, M. Li, Y. S. Cho, M. J. Go, Y. J. Kim, J.-Y. Lee, T. Park, K. Kim, X. Sim, R. T.-H. Ong, D. C. Croteau-Chonka, L. A. Lange, J. D. Smith, K. Song, J. H. Zhao, X. Yuan, J. Luan, C. Lamina, A. Ziegler, W. Zhang, R. Y. L. Zee, A. F. Wright, J. C. M. Witteman, J. F. Wilson, G. Willemsen, H.-E. Wichmann, J. B. Whitfield, D. M. Waterworth, N. J. Wareham, G. Waeber, P. Vollenweider, B. F. Voight, V. Vitart, A. G. Uitterlinden, M. Uda, J. Tuomilehto, J. R. Thompson, T. Tanaka, I. Surakka, H. M. Stringham, T. D. Spector, N. Soranzo, J. H. Smit,

J. Sinisalo, K. Silander, E. J. G. Sijbrands, A. Scuteri, J. Scott, D. Schlessinger, S. Sanna, V. Salomaa, J. Saharinen, C. Sabatti, A. Ruokonen, I. Rudan, L. M. Rose, R. Roberts, M. Rieder, B. M. Psaty, P. P. Pramstaller, I. Pichler, M. Perola, B. W. J. H. Penninx, N. L. Pedersen, C. Pattaro, A. N. Parker, G. Pare, B. A. Oostra, C. J. O'Donnell, M. S. Nieminen, D. A. Nickerson, G. W. Montgomery, T. Meitinger, R. M. Pherson, M. I. Mc Carthy, W. M. Ardle, D. Masson, N. G. Martin, F. Marroni, M. Mangino, P. K. E. Magnusson, G. Lucas, R. Luben, R. J. F. Loos, M.-L. Lokki, G. Lettre, C. Langenberg, L. J. Launer, E. G. Lakatta, R. Laaksonen, K. O. Kyvik, F. Kronenberg, I. R. König, K.-T. Khaw, J. Kaprio, L. M. Kaplan, Å. Johansson, M.-R. Jarvelin, A. C. J. W. Janssens, E. Ingelsson, W. Igl, G. K. Hovingh, J.-J. Hottenga, A. Hofman, A. A. Hicks, C. Hengstenberg, I. M. Heid, C. Hayward, A. S. Havulinna, N. D. Hastie, T. B. Harris, T. Haritunians, A. S. Hall, U. Gyllensten, C. Guiducci, L. C. Groop, E. Gonzalez, C. Gieger, N. B. Freimer, L. Ferrucci, J. Erdmann, P. Elliott, K. G. Ejebe, A. Döring, A. F. Dominiczak, S. Demissie, P. Deloukas, E. J. C. de Geus, U. de Faire, G. Crawford, F. S. Collins, Y.-d. I. Chen, M. J. Caulfield, H. Campbell, N. P. Burtt, L. L. Bonnycastle, D. I. Boomsma, S. M. Boekholdt, R. N. Bergman, I. Barroso, S. Bandinelli, C. M. Ballantyne, T. L. Assimes, T. Quertermous, D. Altshuler, M. Seielstad, T. Y. Wong, E.-S. Tai, A. B. Feranil, C. W. Kuzawa, L. S. Adair, H. A. Taylor Jr., I. B. Borecki, S. B. Gabriel, J. G. Wilson, H. Holm, U. Thorsteinsdottir, V. Gudnason, R. M. Krauss, K. L. Mohlke, J. M. Ordovas, P. B. Munroe, J. S. Kooner, A. R. Tall, R. A. Hegele, J. J. P. Kastelein, E. E. Schadt, J. I. Rotter, E. Boerwinkle, D. P. Strachan, V. Mooser, K. Stefansson, M. P. Reilly, N. J. Samani, H. Schunkert, L. A. Cupples, M. S. Sandhu, P. M. Ridker, D. J. Rader, C. M. van Duijn, L. Peltonen, G. R. Abecasis, M. Boehnke, S. Kathiresan, Biological, clinical and population relevance of 95 loci for blood lipids. *Nature* **466**, 707–713 (2010).

7. J. C. Chambers, W. Zhang, J. S. Sehmi, X. Li, M. N. Wass, P. Van der Harst, H. Holm, S. Sanna, M. Kavousi, S. E. Baumeister, L. Coin, G. Deng, C. Gieger, N. L. Heard-Costa, J. J. Hottenga, B. Kühnel, V. Kumar, V. Lagou, L. Liang, J. Luan, P. M. Vidal, I. M. Leach, P. F. O'reilly, J. F. Peden, N. Rahmioglu, P. Soininen, E. K. Speliotes, X. Yuan, G. Thorleifsson, B. Z. Alizadeh, L. D. Atwood, I. B. Borecki, M. J. Brown, P. Charoen, F. Cucca, D. Das, E. J. de Geus, A. L. Dixon, A. Döring, G. B. Ehret, G. I. Eyjolfsson, M. Farrall, N. G. Forouhi, N. Friedrich, W. Goessling, D. Gudbjartsson, T. B. Harris, A. L. Hartikainen, S. C. Heath, G. M. Hirschfield, A. Hofman, G. Homuth, E. Hyppönen, H. L. Janssen, T. Johnson, A. J. Kangas, I. P. Kema, J. P. Kühn, S. Lai, M. Lathrop, M. M. Lerch, Y. Li, T. J. Liang, J.-P. Lin, R. J. Loos, N. G. Martin, M. F. Moffatt, G. W. Montgomery, P. B. Munroe, K. Musunuru, Y. Nakamura, C. J. O'donnell, I. Olafsson, B. W. Penninx, A. Pouta, B. P. Prins, I. Prokopenko, R. Puls, A. Ruokonen, M. J. Savolainen, D. Schlessinger, J. N. Schouten, U. Seedorf, S. Sen-Chowdhry, K. A. Siminovitch, J. H. Smit, T. D. Spector, W. Tan, T. M. Teslovich, T. Tukiainen, A. Uitterlinden, M. M. Van der Klauw, R. S. Vasan, C. Wallace, H. Wallaschofski, H. E. Wichmann, G. Willemsen, P. Würtz, C. Xu, L. M. Yerges-Armstrong, Alcohol Genome-wide Association (Alc Gen) Consortium, Diabetes Genetics Replication and Meta-analyses (DIAGRAM+) Study, Genetic Investigation of Anthropometric Traits (GIANT) Consortium, Global Lipids Genetics Consortium, Genetics of Liver Disease (GOLD) Consortium, International Consortium for Blood Pressure (ICBP-GWAS), Meta-analyses of Glucose and Insulin-Related Traits Consortium (MAGIC), G. R. Abecasis, K. R. Ahmadi, D. I. Boomsma, M. Caulfield, W. O. Cookson, C. M. van Duijn, P. Froguel, K. Matsuda, M. I. McCarthy, C. Meisinger, V. Mooser, K. H. Pietiläinen, G. Schumann, H. Snieder, M. J. E. Sternberg, R. P. Stolk, H. C. Thomas, U. Thorsteinsdottir, M. Uda, G. Waeber, N. J. Wareham, D. M. Waterworth, H. Watkins, J. B. Whitfield, J. C. M. Witteman, B. H. R. Wolffenbuttel, C. S. Fox, M. Ala-Korpela, K. Stefansson, P. Vollenweider, H. Völzke, E. E. Schadt, J. Scott, M.-R. Järvelin, P. Elliott, J. S. Kooner, Genome-wide association study identifies loci influencing concentrations of liver enzymes in plasma. *Nat. Genet.* **43**, 1131–1138 (2011).
8. E. K. Speliotes, L. M. Yerges-Armstrong, J. Wu, R. Hernaez, L. J. Kim, C. D. Palmer, V. Gudnason, G. Eiriksdottir, M. E. Garcia, L. J. Launer, M. A. Nalls, J. M. Clark, B. D. Mitchell, A. R. Shuldiner, J. L. Butler, M. Tomas, U. Hoffmann, S.-J. Hwang, J. M. Massaro, C. J. O'Donnell, D. V. Sahani, V. Salomaa, E. E. Schadt, S. M. Schwartz, D. S. Siscovick, NASH CRN, GIANT Consortium, MAGIC Investigators, B. F. Voight, J. J. Carr, M. F. Feitosa, T. B. Harris, C. S. Fox, A. V. Smith, W. H. L. Kao, J. N. Hirschhorn, I. B. Borecki, GOLD Consortium, Genome-wide association analysis identifies variants associated with nonalcoholic fatty liver disease that have distinct effects on metabolic traits. *PLOS Genet.* **7**, e1001324 (2011).
9. M. Vujkovic, S. Ramdas, K. M. Lorenz, X. Guo, R. Darlay, H. J. Cordell, J. He, Y. Gindin, C. Chung, R. P. Myers, C. V. Schneider, J. Park, K. M. Lee, M. Serper, R. M. Carr, D. E. Kaplan, M. E. Haas, M. T. MacLean, W. R. Witschey, X. Zhu, C. Tcheandjieu, R. L. Kember, H. R. Kranzler, A. Verma, A. Giri, D. M. Klarin, Y. V. Sun, J. Huang, J. E. Huffman, K. T. Creasy, N. J. Hand, C.-T. Liu, M. T. Long, J. Yao, M. Budoff, J. Tan, X. Li, H. J. Lin, Y.-D. I. Chen, K. D. Taylor, R.-K. Chang, R. M. Krauss, S. Vilarinho, J. Brancale, J. B. Nielsen, A. E. Locke, M. B. Jones, N. Verweij, A. Baras, K. R. Reddy, B. A. Neuschwander-Tetri, J. B. Schwimmer, A. J. Sanyal, N. Chalasani, K. A. Ryan, B. D. Mitchell, D. Gill, A. D. Wells, E. Manduchi, Y. Saiman, N. Mahmud, D. R. Miller, P. D. Reaven, L. S. Phillips, S. Muralidhar, S. L. Du Vall, J. S. Lee, T. L. Assimes, S. Pyarajan, K. Cho, T. L. Edwards, S. M. Damrauer, P. W. Wilson, J. M. Gaziano, C. J. O'Donnell, A. V. Khera, S. F. A. Grant, C. D. Brown, P. S. Tsao, D. Saleheen, L. A. Lotta, L. Bastarache, Q. M. Anstee, A. K. Daly, J. B. Meigs, J. I. Rotter, J. A. Lynch, Regeneron Genetics Center, Geisinger-Regeneron DiscovEHR Collaboration, EPoS Consortium, VA Million Veteran Program, D. J. Rader, B. F. Voight, K.-M. Chang, A multiancestry genome-wide association study of unexplained chronic ALT elevation as a proxy for nonalcoholic fatty liver disease with histological and radiological validation. *Nat. Genet.* **54**, 761–771 (2022).
10. A. K. Manning, A. S. Goustin, E. L. Kleinbrink, P. Thepsuwan, J. Cai, D. Ju, A. Leong, M. S. Udler, J. B. Brown, M. O. Goodarzi, J. I. Rotter, R. Sladek, J. B. Meigs, L. Lipovich, A long non-coding RNA, *LOC157273*, is an effector transcript at the chromosome 8p23.1-*PPP1R3B* metabolic traits and type 2 diabetes risk locus. *Front. Genet.* **11**, 615 (2020).
11. B. Kahali, Y. Chen, M. F. Feitosa, L. F. Bielak, J. R. Oconnell, S. K. Musani, Y. Hegde, Y. Chen, L. C. Stetson, X. Guo, Y. P. Fu, A. V. Smith, K. A. Ryan, G. Eiriksdottir, A. T. Cohain, M. Allison, A. Bakshi, D. W. Bowden, M. J. Budoff, J. J. Carr, S. Carskadon, Y. D. I. Chen, A. Correa, B. F. Crudup, X. Du, T. B. Harris, J. Yang, S. L. R. Kardia, L. J. Launer, J. Liu, T. H. Mosley, J. M. Norris, J. G. Terry, N. Palanisamy, E. E. Schadt, C. J. O'Donnell, L. M. Yerges-Armstrong, J. I. Rotter, L. E. Wagenknecht, S. K. Handelman, V. Gudnason, M. A. Province, P. A. Peyser, B. Halligan, N. D. Palmer, E. K. Speliotes, A noncoding variant near *PPP1R3B* promotes liver glycogen storage and MetS, but protects against myocardial infarction. *J. Clin. Endocrinol. Metab.* **106**, 372–387 (2021).
12. C. G. Armstrong, M. J. Doherty, P. T. W. Cohen, Identification of the separate domains in the hepatic glycogen-targeting subunit of protein phosphatase 1 that interact with phosphorylase a, glycogen and protein phosphatase 1. *Biochem. J.* **336**, 699–704 (1998).
13. R. Gasa, P. B. Jensen, H. K. Berman, M. J. Brady, A. A. DePaoli-Roach, C. B. Newgard, Distinctive regulatory and metabolic properties of glycogen-targeting subunits of protein phosphatase-1 (PTG, G_L, G_M/R_{G1}) expressed in hepatocytes. *J. Biol. Chem.* **275**, 26396–26403 (2000).
14. M. B. Mehta, S. V. Shewale, R. N. Sequeira, J. S. Millar, N. J. Hand, D. J. Rader, Hepatic protein phosphatase 1 regulatory subunit 3B (*Ppp1r3b*) promotes hepatic glycogen synthesis and thereby regulates fasting energy homeostasis. *J. Biol. Chem.* **292**, 10444–10454 (2017).
15. S. Stender, E. Smagris, B. K. Lauridsen, K. F. Kofoed, B. G. Nordestgaard, A. Tybjærg-Hansen, L. A. Pennacchio, D. E. Dickel, J. C. Cohen, H. H. Hobbs, Relationship between genetic variation at *PPP1R3B* and levels of liver glycogen and triglyceride. *Hepatology* **67**, 2182–2195 (2018).
16. N. D. Palmer, S. K. Musani, L. M. Yerges-Armstrong, M. F. Feitosa, L. F. Bielak, R. Hernaez, B. Kahali, J. J. Carr, T. B. Harris, M. A. Jhun, S. L. R. Kardia, C. D. Langefeld, T. H. Mosley Jr., J. M. Norris, A. V. Smith, H. A. Taylor, L. E. Wagenknecht, J. Liu, I. B. Borecki, P. A. Peyser, E. K. Speliotes, Characterization of european ancestry nonalcoholic fatty liver disease-associated variants in individuals of african and hispanic descent. *Hepatology* **58**, 966–975 (2013).
17. R. Hernaez, J. McLean, M. Lazo, F. L. Brancati, J. N. Hirschhorn, I. B. Borecki, T. B. Harris, Genetics of Obesity-Related Liver Disease (GOLD) Consortium, T. Nguyen, I. R. Kamel, S. Bonekamp, M. S. Eberhardt, J. M. Clark, W. H. L. Kao, E. K. Speliotes, E. K. Speliotes, Association between variants in or near *PNPLA3*, *GCKR*, and *PPP1R3B* with ultrasound-defined steatosis based on data from the third national health and nutrition examination survey. *Clin. Gastroenterol. Hepatol.* **11**, 1183–1190.e2 (2013).
18. A.-S. Seidelin, B. G. Nordestgaard, A. Tybjærg-Hansen, S. Stender, Genetic variation at PPP1R3B increases hepatic CT attenuation and interacts with prandial status on plasma glucose. *J. Clin. Endocrinol. Metab.* **105**, dgaa151 (2020).
19. V. L. Chen, X. Du, Y. Chen, A. Kuppa, S. K. Handelman, R. B. Vohnoutka, P. A. Peyser, N. D. Palmer, L. F. Bielak, B. Halligan, E. K. Speliotes, Genome-wide association study of serum liver enzymes implicates diverse metabolic and liver pathology. *Nat. Commun.* **12**, 816 (2021).
20. P. Dongiovanni, M. Meroni, R. M. Mancina, G. Baselli, R. Rametta, S. Pelusi, V. Männistö, A. L. Fracanzani, S. Badiali, L. Miele, S. Grimaudo, S. Petta, E. Bugianesi, G. Soardo, S. Fargion, J. Pihlajamäki, S. Romeo, L. Valenti, Protein phosphatase 1 regulatory subunit 3B gene variation protects against hepatic fat accumulation and fibrosis in individuals at high risk of nonalcoholic fatty liver disease. *Hepatol. Commun.* **2**, 666–675 (2018).
21. R. Gasa, C. Clark, R. Yang, A. A. DePaoli-Roach, C. B. Newgard, Reversal of diet-induced glucose intolerance by hepatic expression of a variant glycogen-targeting subunit of protein phosphatase-1. *J. Biol. Chem.* **277**, 1524–1530 (2002).
22. P. Cohen, The twentieth century struggle to decipher insulin signalling. *Nat. Rev. Mol. Cell Biol.* **7**, 867–873 (2006).
23. L. P. Bechmann, R. A. Hannivoort, G. Gerken, G. S. Hotamisligil, M. Trauner, A. Canbay, The interaction of hepatic lipid and glucose metabolism in liver diseases. *J. Hepatol.* **56**, 952–964 (2012).
24. H.-S. Han, G. Kang, J. S. Kim, B. H. Choi, S.-H. Koo, Regulation of glucose metabolism from a liver-centric perspective. *Exp. Mol. Med.* **48**, e218 (2016).
25. M. Alves-Bezerra, D. E. Cohen, Triglyceride metabolism in the liver. *Compr. Physiol.* **8**, 1–22 (2018).
26. L. Rui, "Energy metabolism in the liver" in *Comprehensive Physiology* (Wiley, 2014), pp. 177–197.

27. J. M. Irimia, C. M. Meyer, C. L. Peper, L. Zhai, C. B. Bock, S. F. Previs, O. P. McGuinness, A. DePaoli-Roach, P. J. Roach, Impaired glucose tolerance and predisposition to the fasted state in liver glycogen synthase knock-out mice. *J. Biol. Chem.* **285**, 12851–12861 (2010).
28. J. M. Irimia, C. M. Meyer, D. M. Segvich, S. Surendran, A. A. Depaoli-Roach, N. Morral, P. J. Roach, Lack of liver glycogen causes hepatic insulin resistance and steatosis in mice. *J. Biol. Chem.* **292**, 10455–10464 (2017).
29. J. D. Browning, J. Baxter, S. Satapati, S. C. Burgess, The effect of short-term fasting on liver and skeletal muscle lipid, glucose, and energy metabolism in healthy women and men. *J. Lipid Res.* **53**, 577–586 (2012).
30. K. L. Donnelly, C. I. Smith, S. J. Schwarzenberg, J. Jessurun, M. D. Boldt, E. J. Parks, Sources of fatty acids stored in liver and secreted via lipoproteins in patients with nonalcoholic fatty liver disease. *J. Clin. Invest.* **115**, 1343–1351 (2005).
31. C. G. Wilson, J. L. Tran, D. M. Erion, N. B. Vera, M. Febbraio, E. J. Weiss, Hepatocyte-specific disruption of CD36 attenuates fatty liver and improves insulin sensitivity in HFD-fed mice. *Endocrinology* **157**, 570–585 (2016).
32. S. R. Nagarajan, M. Paul-Heng, J. R. Krycer, D. J. Fazakerley, A. F. Sharland, X. A. J. Hoy, Lipid and glucose metabolism in hepatocyte cell lines and primary mouse hepatocytes: A comprehensive resource for in vitro studies of hepatic metabolism. *Am. J. Physiol. Endocrinol. Metab.* **316**, E578–E589 (2019).
33. R. G. R. Mooli, S. K. Ramakrishnan, Emerging role of hepatic ketogenesis in fatty liver disease. *Front. Physiol.* **13**, 946474 (2022).
34. N. M. Fong, T. C. Jensen, A. S. Shah, N. N. Parekh, A. R. Saltiel, M. J. Brady, Identification of binding sites on protein targeting to glycogen for enzymes glycogen metabolism. *J. Biol. Chem.* **275**, 35034–35039 (2000).
35. A. Von Wilamowitz-Moellendorff, R. W. Hunter, M. García-Rocha, L. Kang, I. López-Soldado, L. Lantier, K. Patel, M. W. Peggie, C. Martínez-Pons, M. Voss, J. Calbó, P. T. W. Cohen, D. H. Wasserman, J. J. Guinovart, K. Sakamoto, Glucose-6-phosphate-mediated activation of liver glycogen synthase plays a key role in hepatic glycogen synthesis. *Diabetes* **62**, 4070–4082 (2013).
36. D. A. Weinstein, C. E. Correia, A. C. Saunders, J. I. Wolfsdorf, Hepatic glycogen synthase deficiency: An infrequently recognized cause of ketotic hypoglycemia. *Mol. Genet. Metab.* **87**, 284–288 (2006).
37. B. Lu, D. Bridges, Y. Yang, K. Fisher, A. Cheng, L. Chang, Z. X. Meng, J. D. Lin, M. Downes, R. T. Yu, C. Liddle, R. M. Evans, A. R. Saltiel, Metabolic crosstalk: Molecular links between glycogen and lipid metabolism in obesity. *Diabetes* **63**, 2935–2948 (2014).
38. I. López-Soldado, A. Bertini, A. Adrover, J. Duran, J. J. Guinovart, Maintenance of liver glycogen during long-term fasting preserves energy state in mice. *FEBS Lett.* **594**, 1698–1710 (2020).
39. I. López-Soldado, J. J. Guinovart, J. Duran, Increased liver glycogen levels enhance exercise capacity in mice. *J. Biol. Chem.* **297**, 100976 (2021).
40. L. Li, H. Zhou, J. Wang, J. Li, X. Lyu, W. Wang, C. Luo, H. Huang, D. Zhou, X. Chen, L. Xu, P. Li, Metabolic switch from glycogen to lipid in the liver maintains glucose homeostasis in neonatal mice. *J. Lipid Res.* **64**, 100440 (2023).
41. J. Park, M. T. MacLean, A. M. Lucas, D. A. Torigian, C. V. Schneider, T. Cherlin, B. Xiao, J. E. Miller, Y. Bradford, R. L. Judy, Regeneron Genetics Center, A. Verma, S. M. Damrauer, M. D. Ritchie, W. R. Witschey, D. J. Rader, Exome-wide association analysis of CT imaging-derived hepatic fat in a medical biobank. *Cell. Rep. Med.* **3**, 100855 (2022).
42. K. Uehara, W. D. Lee, M. Stefkovich, D. Biswas, D. Santoleri, A. E. Garcia Whitlock, W. J. Quinn III, T. N. Coopersmith, K. T. Creasy, D. J. Rader, K. Sakamoto, J. D. Rabinowitz, P. M. Titchenell, mTORC1 controls murine postprandial hepatic glycogen synthesis via *Ppp1r3b*. *J. Clin. Invest.* **134**, e173782 (2024).
43. K. F. Leavens, R. M. Easton, G. I. Shulman, S. F. Previs, M. J. Birnbaum, Akt2 is required for hepatic lipid accumulation in models of insulin resistance. *Cell Metab.* **10**, 405–418 (2009).
44. J. S. Millar, D. A. Cromley, M. G. McCoy, D. J. Rader, J. T. Billheimer, Determining hepatic triglyceride production in mice: Comparison of poloxamer 407 with Triton WR-1339. *J. Lipid Res.* **46**, 2023–2028 (2005).
45. W.-C. Li, K. L. Ralphs, D. Tosh, Isolation and culture of adult mouse hepatocytes. *Methods Mol. Biol.* **633**, 185–196 (2010).
46. T. E. Akie, M. P. Cooper, Determination of fatty acid oxidation and lipogenesis in mouse primary hepatocytes. *J. Vis. Exp.*, e52982 (2015).
47. K. J. Karczewski, L. C. Francioli, G. Tiao, B. B. Cummings, J. Alföldi, Q. Wang, R. L. Collins, K. M. Laricchia, A. Ganna, D. P. Birnbaum, L. D. Gauthier, H. Brand, M. Solomonson, N. A. Watts, D. Rhodes, M. Singer-Berk, E. M. England, E. G. Seaby, J. A. Kosmicki, R. K. Walters, K. Tashman, Y. Farjoun, E. Banks, T. Poterba, A. Wang, C. Seed, N. Whiffin, J. X. Chong, K. E. Samocha, E. Pierce-Hoffman, Z. Zappala, A. H. O'Donnell-Luria, E. V. Minikel, B. Weisburd, M. Lek, J. S. Ware, C. Vittal, I. M. Armean, L. Bergelson, K. Cibulskis, K. M. Connolly, M. Covarrubias, S. Donnelly, S. Ferriera, S. Gabriel, J. Gentry, N. Gupta, T. Jeandet, D. Kaplan, C. Llanwarne, R. Munshi, S. Novod, N. Petrillo, D. Roazen, V. Ruano-Rubio, A. Saltzman, M. Schleicher, J. Soto, K. Tibbetts, C. Tolonen, G. Wade, M. E. Talkowski, Genome Aggregation Database Consortium, B. M. Neale, M. J. Daly, D. G. MacArthur, The mutational constraint spectrum quantified from variation in 141,456 humans. *Nature* **581**, 434–443 (2020).
48. N. M. Ioannidis, J. H. Rothstein, V. Pejaver, S. Middha, S. K. McDonnell, S. Baheti, A. Musolf, Q. Li, E. Holzinger, D. Karyadi, L. A. Cannon-Albright, C. C. Teerlink, J. L. Stanford, W. B. Isaacs, J. Xu, K. A. Cooney, E. M. Lange, J. Schleutker, J. D. Carpten, I. J. Powell, O. Cussenot, G. Cancel-Tassin, G. G. Giles, R. J. MacInnis, C. Maier, C. L. Hsieh, F. Wiklund, W. J. Catalona, W. D. Foulkes, D. Mandal, R. A. Eeles, Z. Kote-Jarai, C. D. Bustamante, D. J. Schaid, T. Hastie, E. A. Ostrander, J. E. Bailey-Wilson, P. Radivojac, S. N. Thibodeau, A. S. Whittemore, W. Sieh, REVEL: An ensemble method for predicting the pathogenicity of rare missense variants. *Am. J. Hum. Genet.* **99**, 877–885 (2016).
49. J. Park, A. M. Lucas, X. Zhang, K. Chaudhary, J. H. Cho, G. Nadkarni, A. Dobbyn, G. Chittoor, N. S. Josyula, N. Katz, J. H. Breeyear, S. Ahmadmehrabi, T. G. Drivas, V. R. M. Chavali, M. Fasolino, H. Sawada, A. Daugherty, Y. Li, C. Zhang, Y. Bradford, J. E. Weaver, A. Verma, R. L. Judy, R. L. Kember, J. D. Overton, J. G. Reid, M. A. R. Ferreira, A. H. Li, A. Baras, S. A. LeMaire, Y. H. Shen, A. Naji, K. H. Kaestner, G. Vahedi, T. L. Edwards, J. Chen, S. M. Damrauer, A. E. Justice, R. Do, M. D. Ritchie, D. J. Rader, Exome-wide evaluation of rare coding variants using electronic health records identifies new gene–phenotype associations. *Nat. Med.* **27**, 66–72 (2021).
50. J. C. Denny, L. Bastarache, M. D. Ritchie, R. J. Carroll, R. Zink, J. D. Mosley, J. R. Field, J. M. Pulley, A. H. Ramirez, E. Bowton, M. A. Basford, D. S. Carrell, P. L. Peissig, A. N. Kho, J. A. Pacheco, L. V. Rasmussen, D. R. Crosslin, P. K. Crane, J. Pathak, S. J. Bielinski, S. A. Pendergrass, H. Xu, L. A. Hindorff, R. Li, T. A. Manolio, C. G. Chute, R. L. Chisholm, E. B. Larson, G. P. Jarvik, M. H. Brilliant, C. A. Mccarty, I. J. Kullo, J. L. Haines, D. C. Crawford, D. R. Masys, D. M. Roden, Systematic comparison of phenome-wide association study of electronic medical record data and genome-wide association study data. *Nat. Biotechnol.* **31**, 1102–1110 (2013).
51. R. J. Carroll, L. Bastarache, J. C. Denny, R PheWAS: Data analysis and plotting tools for phenome-wide association studies in the R environment. *Bioinformatics* **30**, 2375–2376 (2014).

Acknowledgments: This research has been conducted using the UK Biobank Resource under application number 70653. We thank the University of Pennsylvania Diabetes Research Center (DRC) for the use of the Radioimmunoassay and Biomarkers Core and Metabolic Tracer Resource (P30-DK19525) and the Cardiovascular Institute Histology and Gene Expression Co-Op for histological services. We thank A. Wilson, A. Rodrigues, D. Cromley, and E. Edouard for technical assistance and experimental expertise contributing to this work, and D. Marchadier for helpful discussions and project management. **Funding:** This work was supported by National Institutes of Health grant R01DK114291 (K.T.C., N.J.H., J.A.B., and D.J.R.), National Institutes of Health grant UM1DK126194 (K.T.C., P.M.T., and D.J.R.), National Institutes of Health grant 5R01-DK134575 (M.V.), and American Diabetes Association Postdoctoral Fellowship 1-17-PDF-060 (S.V.S.). **Author contributions:** Conceptualization: K.T.C., M.B.M., S.V.S., N.J.H., P.M.T., J.A.B., and D.J.R. Investigation: K.T.C., M.B.M., C.V.S., J.P., D.Z., J.S.M., and D.J.R. Methodology: K.T.C., M.B.M., S.V.S., M.V., P.M.T., J.A.B., and D.J.R. Visualization: K.T.C. Formal analysis: K.T.C., M.B.M., C.V.S., J.P., D.Z., and M.V. Validation: K.T.C., M.B.M., C.V.S., D.Z., M.V., and D.J.R. Software: C.V.S., J.P., D.Z., and M.V. Resources: C.V.S., S.V.S., J.A.B., and D.J.R. Writing—original draft: K.T.C. and D.J.R. Writing—review and editing: K.T.C., M.B.M., C.V.S., J.P., D.Z., S.V.S., J.S.M., M.V., N.J.H., P.M.T., J.A.B., and D.J.R. Funding acquisition: K.T.C., N.J.H., J.A.B., and D.J.R. Supervision: N.J.H., J.A.B., and D.J.R. Project administration: N.J.H., J.A.B., and D.J.R. **Competing interests:** The authors declare that they have no competing interests. **Data and materials availability:** All data needed to evaluate the conclusions in the paper are present in the paper and/or the Supplementary Materials.

Submitted 28 February 2024
Accepted 10 April 2025
Published 16 May 2025
10.1126/sciadv.ado3440